Title

Legionella uses host Rab GTPases and BAP31 to create a unique ER niche.

Journal

Cell Reports, 43(12)

Authors

Chadha, Attinder
Yanai, Yu
Oide, Hiromu
et al.

Publication Date

2024-12-24

DOI

10.1016/j.celrep.2024.115053

Peer reviewed

HHS Public Access

Author manuscript

Cell Rep. Author manuscript; available in PMC 2025 January 14.

Published in final edited form as:

Cell Rep. 2024 December 24; 43(12): 115053. doi:10.1016/j.celrep.2024.115053.

Legionella uses host Rab GTPases and BAP31 to create a unique ER niche

Attinder Chadha[1,2,5], **Yu Yanai**[4], **Hiromu Oide**[4], **Yuichi Wakana**[4], **Hiroki Inoue**[4], **Saradindu Saha**[1,2], **Manish Paul**[1,2], **Mitsuo Tagaya**[4], **Kohei Arasaki**[4,5,*], **Shaeri Mukherjee**[1,2,3,6,*]

[1]G.W. Hooper Foundation, University of California, San Francisco, San Francisco, CA, USA

[2]Department of Microbiology and Immunology, University of California, San Francisco, San Francisco, CA, USA

[3]Chan Zuckerberg Biohub, San Francisco, CA, USA

[4]School of Life Sciences, Tokyo University of Pharmacy and Life Sciences, Hachioji, Tokyo 192-0392, Japan

SUMMARY

The bacterium *Legionella pneumophila* secretes numerous effector proteins that manipulate endoplasmic reticulum (ER)-derived vesicles to form the *Legionella*-containing vacuole (LCV). Despite extensive studies, whether the LCV membrane is separate from or connected to the host ER network remains unclear. Here, we show that the smooth ER (sER) is closely associated with the LCV early in infection. Remarkably, *Legionella* forms a distinct rough ER (rER) niche at later stages, disconnected from the host ER network. We discover that host small GTPases Rab10 and Rab4 and an ER protein, BAP31, play crucial roles in transitioning the LCV from an sER to an rER. Additionally, we have identified a *Legionella* effector, Lpg1152, that binds to BAP31. Interestingly, the optimal growth of *Legionella* is dependent on both BAP31 and Lpg1152. These findings detail the complex interplay between host and pathogen in transforming the LCV membrane from a host-associated sER to a distinct rER.

In brief

Chadha et al. demonstrate that *Legionella pneumophila* manipulates host cell membranes to form the *Legionella*-containing vacuole (LCV), which is distinct from the host rough ER. This transition is driven by host proteins BAP31, GTPases Rab10 and Rab4, and the *Legionella* effector Lpg1152.

*Correspondence: karasaki@toyaku.ac.jp (K.A.), shaeri.mukherjee@ucsf.edu (S.M.).

[5]These authors contributed equally

[6]Lead contact

AUTHOR CONTRIBUTIONS

K.A. and S.M. conceptualized the study and designed experiments. A.C., K.A., M.P., and S.M. wrote the manuscript. A.C., S.S., K.A., Y.Y., H.O., H.I., M.P., and Y.W. performed experiments. All authors analyzed data. K.A. and S.M. supervised the study. All authors reviewed and approved the manuscript.

DECLARATION OF INTERESTS

The authors declare no competing interests.

SUPPLEMENTAL INFORMATION

Supplemental information can be found online at https://doi.org/10.1016/j.celrep.2024.115053.

Graphical Abstract

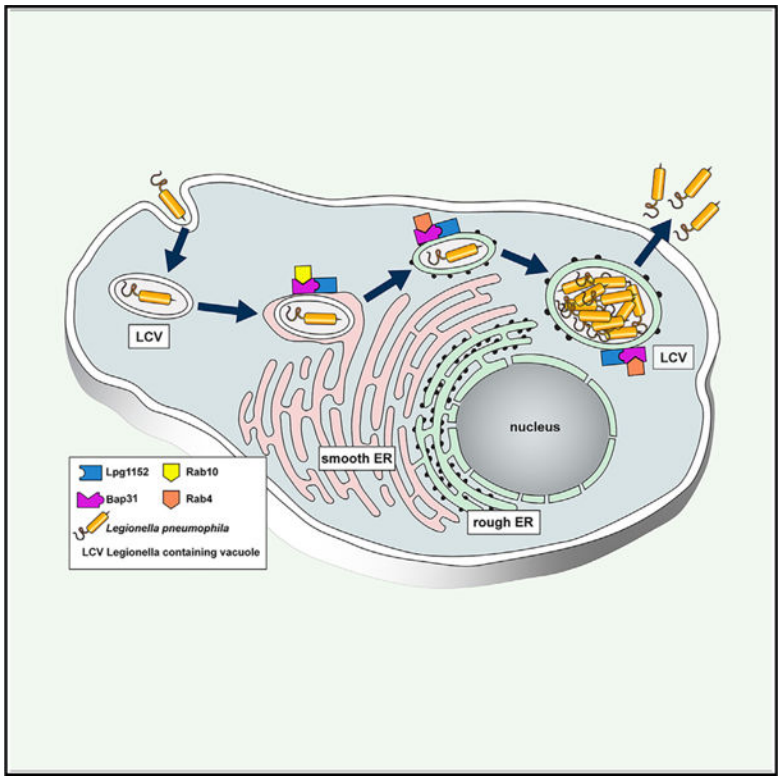

INTRODUCTION

The bacterium *Legionella pneumophila* (*L.p.*) is the causative agent of a severe type of pneumonia known as Legionnaires' disease. *L.p.* primarily affects immunocompromised and elderly patients, and infection can often lead to a high mortality.[1] When aerosols containing *L.p.* are generated, they can enter the human lung, where it is detected and phagocytosed by alveolar macrophages. Upon entry, *L.p.* uses its type IV secretion system, Dot/Icm, to secrete more than 300 bacterial effector proteins into the host cell.[2,3] Despite their identification, the targets and functions of most of these *L.p.* effectors are currently unknown.[4] For the effectors whose functions are known, *L.p.* has been shown to target host proteins that are evolutionarily conserved from amoeba to humans, many of which are key players in regulating membrane traffic in cells.[5–10] Studying the function of *L.p.* effectors has often led to a deeper understanding of the role of essential host proteins, including a novel posttranslational modification[5] and non-canonical ubiquitination signaling.[11–15] Some of these effectors are thought to play key roles in acquiring host endoplasmic reticulum (ER)-derived vesicles to form the *Legionella*-containing vacuole (LCV).[16] Improper ER membrane recruitment leads to defects in bacterial replication.[10,17] However, two big questions remain: (1) is the LCV contiguous with the host ER membrane, or is it a separate entity? (2) What effectors and host proteins help create this unique LCV niche?

The ER is organized into a ribosome binding compartment, termed rough ER (rER), and a non-ribosome binding compartment, termed the smooth ER (sER).[18] The sER has a tubular

structure and functions in Ca^{2+} signaling and lipid synthesis. Its structure is maintained by a wide range of membrane-shaping proteins, including Reticulon-4 (Rtn4).[19] In contrast, the rER has a sheet-like structure and functions in *de novo* protein synthesis.[18] The protein Sec61β functions as a translocon that facilitates protein entry into the ER and is associated with the rER.[20] The composition of the ER membrane, however, is dynamic. This is best characterized by ER-resident proteins that shuttle between sER and rER. One such protein is B cell receptor-associated protein 31 (BAP31).[21] BAP31 is a transmembrane protein that primarily localizes to the sER under steady-state conditions but translocates to the rER under conditions when the ER is perturbed.[22] Due to the continuous exchange of membranes within the ER, the ratio of the rER to the sER in cells is not always constant. This variability in ER sub-compartment composition influences various cellular functions, such as secretory capacity and translation ability.[23] By creating an ER-derived niche, *L.p.* provides an opportunity to explore the intricate communication between different ER sub-compartments.

In this study, we aimed to leverage *L.p.* as a discovery tool to uncover the communication dynamics between ER sub-compartments. Previous observations indicated ribosome presence on the LCV surface, suggesting an rER association.[24] However, recent data show that sER markers such as Rtn4 are ubiquitinated and recruited to the LCV.[25] Here, we try to resolve this seemingly disparate observation by providing evidence that the LCV transitions from an sER association to an rER identity in a temporal manner. Interestingly, it can maintain a unique rER niche that is not contiguous with the host ER membrane. *L.p.* utilizes host Rab GTPases, Rab10 and Rab4, and the ER-resident protein, BAP31, which allow *L.p.* to mature from an sER to an rER identity. Notably, we identify Lpg1152 as a key *L.p.* effector that binds BAP31, facilitating LCV maturation during infection. Thus, our study reveals BAP31 as a Rab effector that is crucial for ER sub-compartment communication, underscoring the elaborate mechanisms by which *L.p.* manipulates host proteins and effectors to rewire the ER network.

RESULTS

L.p. associates temporally with the sER and later creates a unique rER niche independent of the host ER network

Given that *L.p.* has been shown to associate with both sER and rER membranes,[24,25] we sought to understand whether acquiring these markers was a temporally regulated process. We used a HeLa cell line that stably expresses FcγRII (HeLa Fcγ) to facilitate *L.p.* entry via antibody-mediated opsonization. HeLa Fcγ and HEK293 Fcγ are commonly used in *Legionella* research as a surrogate for macrophages due to their superior transfection efficiency and similar outcomes concerning the host processes manipulated by *L.p.* to establish its replicative niche.[5,26,27,28] We analyzed the sER vs. rER association of *L.p.* by confocal microscopy and used Rtn4 and Sec61β as sER and rER markers, respectively. Interestingly, we observed a remarkable temporal segregation of sER and rER markers on the LCV. At the initial stage of infection (2 h), the LCV showed an enrichment of Rtn4 (Figure 1A top panel), suggesting an sER localization. In contrast, at a late stage (8 h), the LCV showed rER association, as evident by Sec61β staining (Figure 1A bottom panel).

These data are consistent with previous EM and confocal data that have demonstrated the enrichment of these markers on the LCV.[25,29,30] Next, we sought to answer a long-standing question in the field: is the LCV membrane separate or contiguous with the host ER membrane? We chose two independent photobleaching techniques to answer this question. First, we employed fluorescence loss in photobleaching (FLIP) time-lapse imaging. Briefly, FLIP is used to assess the continuity between areas within cells and involves the repeated photobleaching of a small region of a cell that expresses a fluorescent marker. Over time, because of the lateral movement of fluorophores, fluorescence loss is seen in other regions of the cell that are interconnected with the bleached area. In contrast, the fluorescence in the unconnected areas is unaffected because fluorescent markers do not pass through the bleached region. We utilized HeLa Fcγ cells that stably express an sER marker (GFP-Rtn4) and an rER marker (RFP-Sec61β). At 3 h post infection, continuous photobleaching of Rtn4 in a region in the ER (red box) which is distant from the LCV membrane (purple box) caused a concomitant loss of the Rtn4 signal both in the host ER network as well as the LCV membrane (Figures 1B and 1C; Video S1), suggesting that the LCV membrane is contiguous with the host sER network. However, at 6 h post infection, even though the photobleaching of Sec61β in ER regions (red box) distant from the LCV (purple box) results in complete loss of fluorescence in the entire host ER membrane, Sec61β fluorescence on the LCV remained mostly protected (Figures 1D and 1E; Videos S2 and S3). The small decrease seen in the first 50 s could be a result of arbitrary drawing of the LCV area. Some peripheral Sec61β staining around the LCV could be rER staining that is associated with the LCV and this signal decreases at the same rate as the rest of the rER signal. The real LCV area is revealed at a later point and shown to be mostly protected from the bleach. This striking result indicates that the ER membrane on the LCV at 6 h post infection is a distinct entity that is independent of the host ER membrane network. To confirm these findings, we subjected HeLa Fcγ cells to fluorescence recovery after photo bleaching (FRAP). FRAP involves the photobleaching of fluorescently tagged proteins via brief, intensive laser excitation followed by measuring the fluorescence recovery rates of the fluorophores back into the briefly bleached area. If the fluorophores are in distinct membrane compartments, there is little recovery. However, interconnected membranes will show recovery of fluorescence over time. After 6 h post infection, photobleaching of Sec61β on the LCV (red box) leads to a significant reduction in fluorescence intensity at the LCV (white arrow) compared to the distal ER (blue box) (Figures 1F and 1G; Videos S4 and S5). By 40 s post bleaching, the host ER (blue box) recovers ~80% of the Sec61β signal, whereas the LCV (red box) only recovers ~20%. This confirms our FLIP findings that, at this late stage, the LCV has a distinct rER membrane separate from the host ER. Taken together, the FLIP and FRAP results unequivocally show that the LCV moves from a host-associated continuous sER membrane to a distinct rER membrane that is independent of the host ER network.

Rab4 and Rab10 facilitate the transition of the LCV from an sER to an rER identity

Our previous results stimulated our interest in identifying molecular mechanisms that facilitate LCV maturation from the sER to the rER. Rab GTPases (members of the Ras superfamily) regulate the maturation of the endosomal and secretory pathway compartments.[31] Indeed, several *L.p.* effectors are known to manipulate and modify these

Rab GTPases.[32] Upon entry, *L.p.* is known to first interact with the endosomal compartment, followed by the acquisition of host ER vesicles.[16] This observation prompted us to ask whether early endocytic and ER-resident Rabs that regulate ER morphology and dynamics[33] and are required for optimal *L.p.* growth[34] are involved in this process.

Earlier work from the Voeltz lab suggested that Rab4 and Rab10 play crucial roles in maintaining ER-endosome contact sites.[33] To assess this, we first confirmed the presence of Rab4 and Rab10 in the ER by subcellular fractionation (Figure 2A). ER-derived membrane fractions (fractions 11–23) were separated from Golgi- and endosome-derived fractions (fractions 1–5). Even though Rab4 and Rab10 were detected in the endosomal fractions (1–3), we also detected a significant amount of Rab4 and Rab10 in fractions containing ER-derived membrane (fractions 11–19) (Figure 2A). Moreover, the separation of rER and sER membranes from whole cell membranes of HEK293 Fcγ cells revealed that Rab10 was predominantly enriched in Rtn4-positive sER, whereas Rab4 was abundant in Sec61β-positive rER (Figure 2B). Indeed, confocal microscopy after 4 h post infection with WT *L.p.* revealed that both Rab4 and Rab10 were associated with the LCV membrane (Figure 2C), suggesting a role for these small GTPases in the LCV maturation process. To test this notion, we silenced Rab4 and Rab10 in HeLa Fcγ cells with small interfering RNAs (siRNAs) (Figure 2D), infected these cells with *L.p.*, and assayed for the association of Rtn4 and Sec61β with the LCV membrane (Figures 2E and 2F). Interestingly, the LCV in Rab10-silenced cells showed dramatic reduction in acquiring either Rtn4 (after 4 h) or Sec61β (after 8 h) (Figures 2E and 2F). In contrast, LCVs in Rab4-silenced cells showed no change in Rtn4 acquisition after 4 h. However, 8 h post infection, Rab4 silencing significantly increased Rtn4-positive vacuoles compared to mock treatment and showed a defect in acquiring Sec61β (Figures 2E and 2F). These results suggested that Rab10 functions upstream of Rab4 during the LCV maturation process and that LCV maturation from sER to rER is at least partly dependent on Rab4 (Figures 2E and 2F). In contrast, recruitment of Sec61β on LCV is downstream of both Rab4 and −10, as silencing of both Rab4 and −10 significantly reduced the vacuoles that were positive for Sec61β at 8 h post infection (Figure 2F). It is also possible that Rab4 is required to remove sER, which sets the stage for rER acquisition.

Given that both Rab4 and −10 are abundant in rER and needed for LCV transition from sER to rER, we next asked whether Rab10 and Rab4 are essential for maintaining the ER sub-compartment architecture. To demonstrate this, Rab10 and Rab4 were silenced in HeLa Fcγ cells and then stained for Rtn4 and Sec61β. Interestingly, silencing of Rab10 disrupted sER morphology (white arrows, Figure 2G), as evident from the less pronounced meshwork of Rtn4 staining in the periphery. These data are consistent with previous literature.[33] Upon Rab4 knockdown, the rER staining (Sec61β) was reduced in the reticular region and appeared to relocate to the periphery, suggesting distorted rER (white solid arrows, Figure 2G). The defective Rtn4 and Sec61β staining has been quantitated and presented as a histogram (Figure 2H). These data point to the crucial role these small GTPase molecules play in maintaining the ER dynamics and morphology. Taken together, these results implicate an interesting temporal kinetics of recruitment of the sER marker on LCV early during infection, followed by the rER. These findings also indicate the involvement of

Rab4 and Rab10 during LCV maturation and their role in maintaining ER sub-compartment morphology.

BAP31 binds to Rab4 and Rab10, while BAP29 interacts with Rab4

Rab proteins act as molecular switches on the membrane and carry out their function with the help of other proteins known as Rab effectors.[31] We reasoned that a Rab effector protein may bind to Rab4 and Rab10 to help facilitate LCV maturation from the sER to the rER. Previous work identified BAP31 as an ER-resident protein that shuttles between the two ER sub-compartments.[22] Furthermore, it was shown to bind to Rab11a, a Rab family member that regulates endocytic recycling.[35] Interestingly, its homolog BAP29, which has ~50% sequence identity with BAP31, resides in the rER and does not shuttle to sER.[36] Together, these data suggest that BAP31 could be a strong candidate to serve as a Rab4/Rab10 effector protein and facilitate LCV maturation.

First, we performed sucrose gradient fractionation to confirm the localization of BAP31 and BAP29 to ER sub-compartments. As reported previously, BAP31 was detected equally in both sER and rER fractions. In contrast, BAP29 was predominantly localized to the rER, with a small fraction also present in the sER (Figure 3A). To demonstrate the *in vivo* interaction of Rab4/10 with BAP31/29, we performed proximity ligand assay (PLA). PLA is used to identify *in vivo* interactions between two proteins within a distance of 30–40 nm. In this assay, cells are fixed and probed with primary antibodies against the proteins of interest. Secondary antibodies with PLA oligonucleotide probes are added that complement each other. A polymerase then amplifies the signal, and fluorescently labeled oligonucleotide probes bind to the amplified DNA. Each signal comprises ~1,000 bound fluorescent probes that appear as punctate dots under a microscope. Interestingly, our results show that BAP31 associates with both Rab4 and Rab10 (Figure 3B), which may partly explain the shuttling of BAP31 between the sER and the rER. Consistent with the localization in the ER subdomain, BAP29 preferentially interacts with Rab4 and less with Rab10 (Figure 3B). These interactions were specific to Rab10 and Rab4 as neither BAP31 nor BAP29 showed any interaction with Rab5 or Rab35 (Figure 3B). The PLA dots have been presented as a histogram (Figure 3C). To further validate these findings, an immunoprecipitation assay was performed. Briefly, HEK293 Fcγ cells were transfected with either 3x-FLAG empty vector (negative control), 3x-FLAG-Rab4, or 3x-FLAG-Rab10 plasmids. Post transfection, cell lysates were immunoprecipitated with a FLAG antibody, and eluates were subjected to SDS-PAGE and immunoblotted with the antibodies against BAP31, FLAG, and BAP29. Consistent with the PLA results, BAP31 immunoprecipitated with both 3x-FLAG-Rab10 and 3x-FLAG-Rab4, whereas BAP29 immunoprecipitated slightly more with 3x-FLAG-Rab4 than with 3x-FLAG-Rab10 (Figures 3D and 3E). These binding studies have been quantitated and presented as a histogram (Figure 3F). Collectively, our results show that BAP31 or BAP29 are interacting partners of Rab4 and Rab10 and perhaps are required for intercompartment shuttling in the ER.

BAP31 is required for the sER-to-rER transition and efficient replication of *Legionella*

Due to the interaction of BAP31 with both Rab10 and Rab4, pivotal players in LCV membrane maturation, we aimed to ascertain *L.p.*'s reliance on BAP31 to facilitate this

crucial process. The initial examination focused on visualizing the recruitment of BAP31 to the LCV membrane. We noted robust recruitment of BAP31 (shown in green within the white box) on the LCV, peaking at 4 h post infection and persisting throughout the 8-h duration (Figure 4A). Subsequently, we hypothesized that BAP31 might be integral to LCV maturation. To explore this hypothesis, we silenced BAP31 in HeLa Fcγ cells using siRNAs (Figure 4B) and infected them with WT *L.p.* for specified durations, followed by immunostaining for Rtn4 (red) and Sec61β (green). Consistent with prior observations, infection of HeLa Fcγ cells treated with mock siRNA demonstrated temporal recruitment of ER markers to the LCV, with Rtn4 peaking at 3 h and Sec61β at 7 h (Figure 4C). In contrast, silencing BAP31 led to an enrichment of Rtn4 (red) on the LCV, accompanied by a depletion of Sec61β (green) (Figure 4D). These findings suggest a crucial role for BAP31 in orchestrating LCV maturation from the sER to the rER. To test if preventing LCV membrane maturation affects *L.p.* replication, we silenced BAP31 and conducted a replicative vacuole assay. BAP31 depletion resulted in a marked reduction in the number of *L.p.* in the LCV (8-h post infection) (Figure 4E). Even at a later time, i.e., 12 h post infection, BAP31 depletion showed a growth defect (Figure 4F). Next, we probed whether recruitment of Rab4/10 and BAP31/29 was dependent on each other during LCV maturation. To do this, first, we checked the recruitment of BAP31 (green) and BAP29 (green) in Rab4- and Rab10-depleted cells. Intriguingly, the silencing of Rab10 impaired the recruitment of BAP31, compared to mock and Rab4 siRNA (Figures S1A and S1B). In contrast, the recruitment of BAP29 was abrogated from both Rab4/10-silenced cells (Figures S1C and S1D). These data further establish the idea that BAP proteins are Rab effectors and are recruited to membranes in a Rab-dependent manner. Next, we explored the dependence of Rab4/Rab10 recruitment to LCVs on BAP31/BAP29 (Figure S2). As expected, Rab10 (red) recruitment on the LCVs was independent of BAP31 and BAP29 (Figures S2A–S2C). However, the recruitment of Rab4 (red) was strongly dependent on BAP31 since silencing of BAP31 caused a dramatic reduction in the mRFP-Rab4-positive vacuoles (Figures S2D and S2E). These results suggest Rab10 and BAP31 play an essential role upstream in recruiting Rab4 and other rER markers to the LCV.

Lpg1152 binds BAP31 and is required for optimal LCV maturation

L.p. secretes over 330 effector proteins into the host cytosol; thus, finding the effector that binds to BAP31 is not trivial. We took advantage of *L.p.* strains that lack five large genomic island clusters and hence lack about ~70 effectors[37] (Figure 5A). Δ*P* is a pentuple strain lacking all five clusters (Δ*2ab*, Δ*3*, Δ*4a*, Δ*6a*, and Δ*7a*). To identify the effector(s) that are required for the recruitment of BAP31 on LCV, we analyzed WT, Δ*dotA* (which lacks the entire secretion system), Δ*P* (pentuple, which lacks all five clusters), and individual genomic cluster deletion strains (Δ*2ab*, Δ*3*, Δ*4a*, Δ*6a*, and Δ*7a*) of *L.p.* Excitingly; we found that BAP31 was not recruited on LCVs in the Δ*dotA*, Δ*P*, and Δ*2ab* genomic strain, suggesting that one or more effector(s) present in the Δ*2a* region is required for the BAP31 recruitment on the LCVs (Figure 5B). No change was observed in the recruitment of BAP31 on LCVs from other cluster deletion strains, which includes Δ*3*, Δ*4a*, Δ*6a*, and Δ*7a* (Figure 5B), indicating that effectors from these regions are not essential for BAP31 recruitment. Further analysis of all the effectors on this island led to identifying a single effector, Lpg1152, that coimmunoprecipitated with BAP31 (Figure S3A). To confirm that

Lpg1152 is an ER-localized protein, HeLa cells were transfected with 3xFLAG-Lpg1152, and immunofluorescence microscopy was performed with an anti-BAP31 antibody to detect endogenous BAP31. As expected, BAP31 colocalized with Lpg1152 (Figure 5C). Next, we set out to determine whether Lpg1152 interacts with BAP31 and BAP29. To this end, HEK293 Fcγ cells were transfected with either a 3X-FLAG vector (negative control) or 3x-FLAG-Lpg1152, followed by a co-immunoprecipitation (coIP) using an FLAG tag antibody. Endogenous BAP31 and BAP29 were then immunoblotted. Surprisingly, only BAP31 but not BAP29 interacted with Lpg1152 (Figures 5D and 5E). To get a better understanding of the interaction between Lpg1152 and BAP31, we employed two techniques. First, we purified BAP31 and Lpg1152 from bacterial cells and found that this interaction could be recapitulated *in vitro* (Figures S3B and S3C). Next, we used *in silico* analysis (see STAR Methods) to determine the structures of BAP31 and Lpg1152. The amino acid sequences of Lpg1152 (Uniprot: Q5ZWD3) and BAP31 (Uniprot: P51572) retrieved from UniProtKB had 318 and 246 residues, respectively. Visualization of the 3D structure obtained from AlphaFold showed many unstructured portions without any proper folds (Figure S4A). BAP31 had two solved X-ray crystallographic structures (PDB: 4JZL, 4JZP) (Quistgaard et al.[38]), but the structure for this protein is available for a very small region only (Figure S4C). Three-dimensional structural features obtained from our molecular modeling showed that both Lpg1152 and BAP31 have cytosolic domain, transmembrane region, and extracellular region (Figures S4B and S4D). We identified two sets of significant conformational ensembles for Lpg1152 and BAP31 proteins (Figure S5). Results obtained from the molecular docking revealed that Lpg1152 interacts with BAP31 via residues from its C-terminal region that spanned the extracellular and membrane-bound regions of BAP31 (Figure 5F). The electrostatic potential surface of BAP31-binding groove in Lpg1152 shows that the protein-protein interface is abundant in hydrophobic residues (Figure 5G). Residues ranging from Gln236 to Ala277 in Lpg1152 are shown to make interactions with the residue patch (Tyr13-Arg101) of BAP31 (Figure 5H; Table S3). According to the docking score, the docked complexes between Lpg1152 and BAP31 can be arranged in the following order as per the decreasing binding affinity between the two interacting proteins: dock 1 (−301.6) > dock 3 (−290.2) > dock 2 (−267.76) > dock 4 (−263.39) (Table S4).

Finally, to test whether Lpg1152 drives BAP31 recruitment to the LCV, we generated a Δ*lpg1152* strain and a complemented Δ*lpg1152::*3xFLAG-Lpg1152 strain. First, we confirmed that there is no significant difference in the infection efficiency of these mutant strains (Figure 5I). As expected, the Δ*lpg1152* strain showed a marked reduction in the recruitment of BAP31 to LCVs after 4 h post infection (Figure 5J). However, the recruitment of BAP31 to LCVs was restored with the Lpg1152 complemented strain (Δ*lpg1152::3xFLAG-Lpg1152*), suggesting a role for Lpg1152 in recruiting BAP31 to LCVs (Figure 5J). Surprisingly, we observed partial restoration of BAP31 recruitment to LCVs after 6 h of *Δlpg1152* infection, indicating that Lpg1152 is required for BAP31 recruitment early during infection (Figure 5J). Perhaps other redundant effectors or Rab10 alone may be sufficient to recruit BAP31 later during infection. It is common for *Legionella* to secrete several functionally redundant effectors to carry out the same function.[37] Given that Lpg1154 also binds BAP31 (albeit less efficiently than Lpg 1152), this could be a distinct possibility (Figure S3A). Next, we explored the role of Lpg1152 in recruiting sER

and rER markers to LCVs. To this end, HeLa Fcγ cells were infected with WT, Δ*dotA*, Δ*lpg1152*, and Δ*lpg1152::3xFLAG-Lpg1152* strains, and cells were scored for the vacuoles positive with the sER and rER markers (Rtn4 and Sec61β). As expected, the Δ*lpg1152* strain showed enhanced recruitment of Rtn4 over Sec61β, suggesting a defect in transition to the rER 8 h post infection (Figure 5K). In contrast, infection of HeLa Fcγ cells with D*lpg1152::*3xFLAG-Lpg1152 *L.p.* strain restored the recruitment of Rtn4 and Sec61β to the WT *L.p.* infection levels (Figure 5K). Finally, we elucidated the role of Lpg1152 in the replication of *Legionella* in HeLa Fcγ and U937 macrophage-like cells. We found that replication of the Δ*lpg1152 L.p.* strain was significantly inhibited in both cell types (Figures 5L and 5M). Notably, these phenotypes were rescued by Δ*lpg1152::3xFLAG-Lpg1152* WT strain, suggesting that Lpg1152 is required for optimal replication of *L.p.* Collectively, these results point to a role for Lpg1152 in LCV maturation and replication.

BAP29 plays an antagonistic role to syntaxin 18 in maintaining sER and rER boundaries

We were intrigued by our finding that, while BAP31 and BAP29 share 50% homology, *L.p.* effector Lpg1152 specifically interacted with BAP31 and not BAP29. Even though it was known that BAP31 and BAP29 form a complex,[39] the function of BAP29 remains undefined. Here, we uncovered a role of BAP proteins as Rab effectors that facilitate the transition of the LCV from the sER to the rER. Given that BAP31 shuttles between the sER and rER, but BAP29 does not, we wondered whether BAP29 functions independently of BAP31. To address this, we first examined whether loss of BAP29 affects ER sub-compartment morphology. Typically, Sec61β, mainly seen on rER, is observed as a perinuclear sheet-like structure separated from the peripheral tube-like structure of sER (Rtn4). We observed this staining in mock or BAP31-silenced cells. However, when BAP29 is silenced, a significant distribution of Sec61β to peripheral tube-like structure that overlaps with Rtn4 was observed (white arrow, Figure 6A), suggesting that compartmentation between sER and rER is collapsed when BAP29 is absent. Thus, BAP29 might play an independent role in maintaining rER/sER identity. To gain more critical insight into the BAP29 function, we next examined the effect of dysfunction of BAP29 on the patch-like structure of sER induced by silencing syntaxin 18 (Stx18).[40] Stx18 was initially identified as an sER-localized soluble NSF attachment receptor (SNARE) and is known to maintain the organization of ER subdomains and ER exit sites.[40] Previous studies showed that the architecture of sER is drastically changed from tube-like to patch-like structure when Stx18 is depleted.[40] Consistent with this, we observed a similar patch-like structure of Rtn4 where it was separated from Sec61β when Stx18 was silenced (Figure 6B). Given that this phenotype is thought to be caused by segregation of sER and rER, we hypothesized that additional depletion of BAP29 could restore the phenotype as it would promote mixing of sER with rER. To test this, we knocked down Stx18 alone (Figures 6C and 6D) or in combination with BAP29 or BAP31 (Figure 6E). In these conditions, the patch-like structure of sER marked by Rtn4 was observed in cells silencing Stx18 alone or both Stx18 and BAP31 (Figure 6E). Notably, in cells where both BAP29 and Stx18 were depleted, the distribution pattern of Rtn4 was restored entirely from a patch-like to a tube-like structure (Figure 6E), indicating that BAP29 plays a crucial role in the regulation of the boundary between sER and rER, and this function is independent of BAP31.

DISCUSSION

Throughout history, pathogens have served as valuable tools for unraveling the intricacies of basic cell biology.[41] In recent years, *L.p.* has emerged as particularly insightful in this regard.[42] While previous studies have indicated *L.p.*'s residence in an ER-like compartment, the localization of both sER and rER markers within this compartment has presented conflicting interpretations.[24,25] Moreover, the question remains whether this compartment is an integral part of the host ER or constitutes a distinct entity altogether. Recent data show that *L.p.* modifies the sER protein (Rtn4) with a non-canonical ubiquitin modification, which further adds to the intrigue as to what the identity of LCV really is.[25] Although most pathogens enter the ER through retrograde trafficking, our use of FLIP and FRAP shows that *L.p.* does not reside within the host ER but establishes the LCV by acquiring the ER membrane. To our knowledge, this is a unique manner of establishing an ER-like compartment and begs the question of what the benefits of creating a separate compartment are instead of utilizing the existing host compartment. Additionally, recent studies suggest that obesity can induce significant changes in ER sub-compartmentalization, characterized by ER sheet disorganization and proliferation of ER tubules.[43] Our discovery provides a platform for future studies into the physical remodeling of the ER membrane, which in turn could improve our understanding of processes such as ERphagy and stress-induced membrane remodeling.

Here, we describe a mechanism whereby *L.p.* diverges from the conventional retrograde trafficking route to co-opt the small GTPases Rab10 and Rab4, thus establishing an autonomous ER-like replicative niche, the LCV. We show that the knockdown of the small GTPase Rab10 prevents the LCV from acquiring ER identity, and the knockdown of Rab4 prevents the maturation of this compartment from sER to rER. This is consistent with previous data that show that Rab10 is required for optimal *L.p.* growth.[34] Additionally, we elucidate that, while this niche initially adopts an sER identity, *L.p.* orchestrates its maturation into rER through the actions of the proteins BAP31 and BAP29. These findings not only advance our understanding of *L.p.* pathogenesis but also shed light on fundamental aspects of cellular biology, highlighting the dynamic interplay between pathogens and host cells.

Furthermore, we demonstrate that the *L.p.* effector Lpg1152 binds to and recruits the host protein BAP31 to the LCV. While prior work showed that BAP31 shuttles between sER and rER,[22] our data establish that it functions as a Rab effector to impart sub-compartment identity. Indeed, knocking down BAP31 prevents the LCV from acquiring rER identity. We also show that the BAP31 homolog BAP29 resides on the LCV in a Rab10- and Rab4-dependent manner. While much less is known about BAP29 than BAP31, here, we discover a role in maintaining sER and rER continuity in a syntaxin18-dependent manner.

Our findings elucidate molecular players that define ER sub-compartment identity and facilitate the transition from sER to rER. This exciting finding further opens the possibility of exploring new mechanisms as to how a cell maintains its sER-rER ratio at any given time. Depending on the cell type, cells can have diverse protein and lipid synthesis needs. Thus, maintaining a correct sER-rER boundary can be vital for optimal cell function. Future work

will help determine how separate compartmentalization benefits the pathogen and could lead to an improved understanding of the machinery and mechanisms involved in defining and remodeling ER sub-compartments.

Limitations of the study

Our study has a few limitations that are important to acknowledge. First, while we demonstrate that Lpg1154 binds to BAP31, this interaction is less efficient compared to Lpg1152, and we did not delve into the detailed dynamics of this binding. We recognize that understanding how this interaction influences *L.p.* growth could provide valuable insights and should be explored in future research. Second, we faced technical challenges in validating the Lpg1152-BAP31 interaction during infection due to the relatively small amount of Lpg1152 secreted by *L.p.* Third, we did not identify the specific residues in Lpg1152 that interact with BAP31. Although our *in silico* analysis indicated a potential region of amino acids in the C terminus, we were unable to validate these findings experimentally. Further investigation into these aspects could be a promising avenue for future studies.

RESOURCE AVAILABILITY

Lead contact

Further information and requests for resources and reagents should be directed to and will be fulfilled by the lead contact, Shaeri Mukherjee (Shaeri.Mukherjee@ucsf.edu).

Materials availability

All materials generated in this study are available from the lead contact.

Data and code availability

- No new datasets have been generated in this study that need deposition.
- This paper does not report an original code.
- Any additional information required to reanalyze the data reported in this paper is available from the lead contact upon request.

STAR★METHODS

EXPERIMENTAL MODEL AND STUDY PARTICIPANT DETAILS

Cell lines—HeLa, HeLa cells stably expressing the Fcγ receptor IIb (HeLa Fcγ cells) (a kind gift from the lab of Dr. Craig Roy at Yale University), HEK293 Fcγ, and HeLa Fcγ cells expressing GFP-Rtn4 and RFP-Sec1β were cultured in Dulbecco's Modified Eagle's Medium media (DMEM, GIBCO). U937 cells were cultured in RPMI −1640 (Corning) media. DMEM and RPMI-1640 media were supplemented with 10% heat-inactivated fetal bovine serum (FBS, VWR). U937 cells (a kind gift from Dr. Michael Bassik at Stanford University) were differentiated into macrophage-like cells using 20 ng/ml phorbol 12-myristate 13 acetate (PMA, Sigma) for 72 h, and cells were replated in media without PMA and allowed to recover for 72 h before *Legionella pneumophila* (*L.p*) infection.

Cell line validation and mycoplasma testing—Studies have shown that 18–36% of cell lines are incorrectly identified. UC Berkeley offers investigators short tandem repeat finger-printing of human cell lines by our Genomics Shared Resource at a subsidized cost of $60 per sample that includes reporting the best match. We test cell lines when they first enter the laboratory except for a reliable cell line supplier (e.g., ATTC) when they are brought out of the freezer and at 4-month intervals during the passage. Wherever possible, we attempt to use panel cell lines and avoid basing wide-ranging conclusions on a small number of cell lines. Contamination of cell cultures by mycoplasma remains a major problem in cell culture. We routinely test all cell line cultures every month for mycoplasma contamination by PCR as a service of our Genomics Shared Resource.

Bacterial strains and infection—*Lp01* WT and the isogenic D*dotA* strains are a kind gift from Dr. Craig Roy (Yale University). *Lp02* WT and the isogenic pentuple and individual genomic deletion cluster strains were kind gifts from Dr. Ralph Isberg (Tufts University). All L.*p.* strains were grown on charcoal yeast extract (CYE) agar plates supplemented with iron ($FeNO_3$ 0.135g/10mL) and cysteine (0.4g/10mL). Chloramphenicol (10 mg/mL), IPTG (0.1mM), and thymidine (100 μg/mL) were added to CYE agar plates as needed. For infection experiments, primary patches of *L.p.* were grown for 2 days at 37°C on CYE plates. Single colonies of bacteria were picked and grown as heavy patches for 2 further days on CYE plates at 37°C. Heavy patches were then harvested, diluted in AYE broth supplemented with the required chemicals (as appropriate), and grown overnight at 37°C with shaking (220rpm) until the OD_{600} = ~3. HEK293 Fcγ cells were infected at a multiplicity of infection (MOI) of 50 or 5. For opsonization, *L.p.* bacteria were diluted in complete media and mixed with a *Legionella* polyclonal antibody (Invitrogen, Cat #PA1–7227) at 1:1,000 dilution. The mixtures were then incubated for 20 min at room temperature in a rotary mixer. Immediately after the addition of the opsonized *L.p.* mixtures, cells were centrifuged for 5 min at 1,000 rpm to facilitate spin-fection. Cells were then incubated at 37 °C for 60 min to allow bacterial uptake via the Fcγ receptor. After 60 min, the cells were washed with 1x PBS to remove extracellular bacteria and replenished with DMEM supplemented with 10% FBS. Infected cells were then cultured at 37 °C until the time of harvest.

METHOD DETAILS

Immunofluorescence—HeLa Fcγ cells were seeded on 15mm glass coverslips in 12-well plates and transfected with indicated expression plasmids. 24 h post-transfection, cells were washed with PBS and infected with *L.p.* at MOI = 10. One hour post-infection, cells were washed twice with PBS to remove unwanted extracellular bacteria. Following infection for the indicated times, cells were washed twice with PBS, fixed in 4% paraformaldehyde in PBS for 15 min at room temp. After fixation, extracellular bacteria were stained. Cells were then permeabilized with 0.2% Triton X-100 in PBS, blocked in 2% bovine serum albumin (BSA) in PBS, and incubated with the indicated primary and secondary antibodies diluted in the blocking solution. Coverslips were mounted with ProLong Diamond Antifade Mountant with DAPI (Thermo Fisher Scientific) to stain host and bacterial nucleic acid.

FLIP-FRAP—HeLa Fcγ cells stably expressing GFP-Rtn4 and RFP-Sec61β were infected with Halo-tagged WT *L.p.* for the indicated times. FRAP and FLIP techniques were used to photo bleach the sER marker Rtn4 (green) or the rER marker (red) Sec61β. For the FLIP experiment, the cell's marked region (dotted squares) was photobleached every 10 s for 120 s, and timelapse images were taken every 1 s. For FRAP, the highlighted cell region was photobleached every 0.5 s for 40 s, and timelapse images were taken every 1-s post-bleaching.

Proximity ligand assay (PLA)—Reagents of PLA were purchased from Sigma-Aldrich, and the assay was conducted according to the manufacturer's protocol.

CFU assay—U-937 cells were stimulated with PMA (20 ng/ml) for 72 h and seeded in triplicates at 3×10^5 cells/well density. Post 72-h PMA incubation, cells were washed with PBS and infected with WT, D*dotA*, D*lpg1152*, and D*lpg1152*:3X-FLAGLpg1152 strains of *L.p* for 1 h (Day 0), 24 h (Day 1), 48 h (Day 2), and 72 h (Day 3). One hour post-infection, cells were washed with PBS containing gentamycin (100 mg/ml) to kill extracellular bacteria. After washing the cells with PBS, DMEM media containing gentamycin (100 mg/ml) was added to wells for 45 min, and the cells were again washed three times with PBS. Post PBS washing, media was added back to wells, and cells were allowed to proceed for infection for the times mentioned earlier. Following infection, cells were lysed in 1 mL H_2O and plated on CYE plates (with serial dilutions). Note: Only undiluted samples were used for the Δ*dotA* strain of *L.p.* since these mutants are defective in growth.

Replicative vacuole assay—HeLa Fcγ cells were transfected without or with siRNA against BAP31. At 72 h after transfection, cells were infected with wild-type *L.p.* for 8 h and fixed, stained with anti-*L.p.* antibody for detection of extracellular *L.p.,* permeabilized with 0.2% Triton X-100, and restained with DAPI for detection of intracellular bacteria. The number of intracellular *L.p.* in each vacuole was scored.

Immunoprecipitation—HEK293 Fcγ cells were seeded in 6-well plates and transfected with the indicated plasmid (3x-FLAG vector, 3x-FLAG-Rab4, 3x-FLAG-Rab5, 3x-FLAG-Rab10, or 3x-FLAG-Lpg1152). Post 24 h, cells were washed with PBS and lysed in 300 μL of cell lysis buffer (150mM KCl, 25 mM Hepes-KOH pH7.4, 1% Triton X-100, protease inhibitor cocktail) on ice for 20 min. Lysates were spun down at 15,000 rpm for 10 min at 4°C, and detergent soluble supernatant fraction was collected and designated as cell lysate. Cell lysates were incubated with anti-FLAG M2 affinity beads (Sigma-Aldrich) for 1 h at 4°C. After incubation, beads were washed three times with lysis buffer not containing the inhibitor cocktail, and the bound proteins were eluted by adding 20 μL of Laemmeli buffer and boiling for 5 min at 100°C.

Western blotting—Sample-loaded SDS-gels were transferred onto the PVDF membrane (Merck-Millipore), and membranes were blocked in 5% milk or 2% BSA in TBS containing 0.1% Tween 20 (TBS-T) for 1 h at room temp. After blocking, membranes were incubated with primary antibodies for 1 h at room temp or overnight at 4°C, washed with TBS-T three times, and incubated with horseradish peroxidase (HRP)-conjugated secondary

antibodies (Bio-Rad) for 1 h at room temp. The HRP signal was detected using an enhanced chemiluminescence reagent (Merck-Millipore).

RNA interference—RNA duplexes used for targeting were Rab4 (5′-AACCTACAATGCGCTTACTAA-3′), Rab10 (5′-AAGAGTTGTACCTAAAGGAAA-3′), BAP29 (5′-AACTAAAAAGGATTTTGAAAA-3′), and BAP31 (5′-CAGCACTAAGCAAAAACTAGA-3′). RNA duplex used for targeting Stx18 was described previously. The RNA duplexes were purchased from Japan Bioservice, Inc. Transfection of the RNA duplexes was performed at a final concentration of 200 nM using Oligofectamine (Thermo Fisher Scientific) according to the manufacturer's protocol.

Subcellular fractionation—About 90% confluent HeLa Fcγ cells (three 15 cm dishes) were washed twice in PBS and then once in homogenization buffer (10 mM Hepes-KOH (pH7.4), 0.25 M sucrose, 1 mM EDTA, and protease inhibitor cocktail). After washing, cells were collected, suspended in 1 mL of homogenization buffer, and then homogenized by passaging 15 times through a 26G needle. The homogenate was centrifuged at *1,000* × *g* for 10 min, and the resulting post-nuclear supernatant (PNS) was layered onto a 0–28% OptiPrep (Abbott Diagnostic Technologies) continuous gradients and centrifuged at *200,000* × *g* for 6 h. After centrifugation, 24 fractions (170 μL each) were collected from the top to bottom.

Isolation of the smooth and rough ER fractions—Homogenate preparation from HeLa Fcγ cells (from five 15 cm dishes) was prepared as described above. After preparation of the PNS fraction, the PNS fraction was centrifuged at 10,000 × g for 10 min to remove the mitochondrial fraction. Then, the supernatant was additionally centrifuged at *100,000* × *g* for 1 h. The resulting pellet (total membrane fraction) was suspended in 1.5 mL homogenization buffer. The sucrose concentration of suspension was adjusted to 1.17 M by adding 2 M sucrose in homogenization buffer, and then 1.1 mL of suspension was overlaid on gradients of 1.1 mL of 1.15 M sucrose, 1.4 mL of 0.86 M sucrose, and 1.1 mL of 0.25 M sucrose in homogenization buffer. The gradients were centrifuged at *100,000* × *g* for 3 h, and then the two fractions, the smooth ER fraction at the upper portion of 1.17 M sucrose phase and the rough ER pellet were obtained. The membrane of the smooth ER fraction was collected by centrifugation at 100,000 × g for 1 h, and the smooth ER pellet and the rough ER pellet were resuspended in a homogenization buffer.

Amino acid sequence retrieval and structure prediction—Amino acid sequence of *Legionella pneumophila* subsp. *pneumophila* (strain Philadelphia 1/ATCC 33152/DSM 7513) protein Lpg1152, (Uniprot ID: Q5ZWD3) was retrieved from UniProtKB resource (https://www.uniprot.org/). The sequence was submitted to the I-TASSER server (Yang et al.[50]) for a three-dimensional model prediction of the Lpg1152 protein. The models are generated through a combinatorial process of threading, ab initio modeling, and structure refinement. The local accuracy of the model was determined by ResQ (Yang et al.[51]) prediction in I-TASSER. In this prediction, support vector regression was used for calculating the coverage of threading alignment, divergence of I-TASSER simulation decoys, and determination of sequence-based secondary structure and solvent accessibility.

The 3D model structure of human BAP31 (Uniprot ID: P51572) was predicted in Swissmodel server (Waterhouse et al.[52]) based on a previously determined 3D model of the same protein in Alphafold (Varadi et al.[53]).

Analysis of structural domains in protein—Domains present in the 3D structures of Lpg1152 and BAP31 were determined by the InterProScan database (Paysan-Lafosse et al.[54]). InterProScan allows submitted sequences to be scanned against InterPro's member database signatures such as CATH, CDD, HAMAP, MobiDB Lite, Panther, Pfam, PIRSF, PRINTS, Prosite, SFLD, SMART, SUPERFAMILY and NCBIfam.

Clustering of modeled structures for significant conformational ensembles—To discover significant conformational ensembles, both the 3D model structures of Lpg1152 and Bap31 were submitted in WebGro online tool (https://simlab.uams.edu/) for performing a 50 ns molecular dynamics (MD) simulation. In WebGro, all the MD simulations were performed using GROMOS96 43a1 force field (GROMOS96). The 3D models were solvated in a cubic box containing the SPC water model (Miyamoto.[55]). All protein atoms were maintained at a distance equal to 1.0 nm from the box edges. For neutralizing the net charge of the system, 0.15 M sodium chloride (NaCl) was added. The solvated and neutralized systems were then subjected to energy minimization for 5000 steps by the steepest descent integrator. After performing energy minimization, both the minimized systems were equilibrated for 100 ps at 300 K temperature by position-restrained MD simulation in order to maintain a constant pressure and temperature of systems and relax the solvent. Following equilibration, both systems were then subjected to final MD simulations for 50 ns each at 300 K temperatures.

For the clustering of significant conformational ensembles, principal component analysis (PCA) of the two simulated systems was performed from the trajectories obtained from the MD simulation. During PCA, covariance matrices of the positional fluctuations of the protein's Ca atoms, as well as quantitative characterization of protein dynamism were analyzed. The covariance matrices were diagonalized by two eigenvectors, principal component 1 (PC1) and principal component 2 (PC2). The covariance matrix provides information about the correlated motions of the protein backbone throughout the simulation trajectory. Using this covariance matrix, significant conformational ensembles throughout the simulation trajectory were identified for Lpg1152 and BAP31 protein. Conformational ensembles for Lpg1152 and BAP31 were identified throughout the MD simulation trajectories for each of those proteins by merging the PC1 and PC2 eigenvalues. The average 3D structures from each of the set of conformational ensembles were extracted within the identified time scale range for Lpg1152 and BAP31. The average structures were allowed energy minimization using steepest descent integrator in the GROMACS 5.1.2 (Páll et al.[56]) and GROMOS96(GROMOS96). 43a1 force field was implemented on Intel Xeon Quad Core W3530 2.8 8M 1366 Processor with LINUX.

Molecular docking between Lpg1152 and BAP31—The conformers of Lpg1152 and BAP31 obtained from the clustering of MD simulation trajectories were subjected to molecular docking in HDOCK server (Yan et al.[57]) (http://hdock.phys.hust.edu.cn/). A set of docking has been performed in this server considering the combination of all

the significant conformations obtained the clustering of MD simulation trajectories. The server also calculated the docking score, confidence score and ligand RMSD as well for all the docked complexes. The XMGrace (Vaught.[58]) tool provided by GROMACS program package was utilized to analyze the conformational ensembles obtained throughout MD trajectories. PyMOL (https://www.pymol.org/) was used to analyze the structural features of the modeled proteins, highlighting the protein-protein interface residues.

Recombinant protein purification—Protein-protein interaction studies were conducted *in vitro* using purified recombinant proteins. Human BAP31 was cloned into the pGEX-6P-1 vector containing a GST tag, while LPG1152 was cloned into the pMAL-c5X vector with an MBP tag. Briefly, GST-Bap31 and MBP-Lpg1152 were overexpressed in E. coli BL21(DE3) strain until OD600 of 0.6 was achieved. Protein expression was induced by adding 1 mM isopropyl-b-*d*-thiogalactoside (IPTG) at 37°C for 3 h and at 16°C for 10 h, respectively. Post IPTG induction, the bacterial cultures were centrifuged at 6,000 rpm for 5 min at 4°C, and the pellets were resuspended in bacterial lysis buffer (50 mM Tris pH 8, 100 mM NaCl, 1 mM EDTA, 200 μg/mL lysozyme, 2 μM DTT, 10 mg/mL DNase, and protease inhibitors) for 60 min on ice. The samples were then sonicated on ice (30 s on, 30 s off, 30% amplitude, for 5 min) and centrifuged at 15,000g for 30 min at 4°C. GST alone or GST-Bap31 was purified using glutathione sepharoseTM 4B beads (GE Healthcare), and MBP alone or MBP-Lpg1152 was purified with amylose resin (New England BioLabs), following the manufacturers' protocols. Purified protein fractions were analyzed by SDS-PAGE, and only fractions with high purity were selected for further experiments. For the protein-protein interaction assay, 0.5 mM of each protein (either alone or in combination) was incubated overnight at 4°C followed by incubation with amylose resin at 4°C for 1.5 h. Post incubation with amylose resins, samples were washed three times with the wash buffer (PBS +0.1% Tween 20) to remove unbound proteins. The eluted samples were run onto the SDS-PAGE and subjected to western blotting using antibodies against MBP (Proteintech #66003-1-Ig) and GST tags (Proteintech #66001–2-Ig). Furthermore, Coomassie Brilliant Blue staining was performed to visualize the input lanes.

QUANTIFICATION AND STATISTICAL ANALYSIS

GraphPad Prism version 10 was used to draw all graphs and conduct all statistical analyses. The statistical details of all experiments are described in the figure legends.

Supplementary Material

Refer to Web version on PubMed Central for supplementary material.

ACKNOWLEDGMENTS

We thank Dr. Hana Kimura and Dr. Ady Steinbach for generating *L.p.* knockout (D*lpg1152*) and complemented strains (D*lpg1152*::*3xFLAG-Lpg1152*) and conducting preliminary experiments with them. We thank Dr. Advait Subramanian and Tom Moss for critically reading and editing the manuscript. We thank Dr. Hana Kimura and the Center For Advanced Light Microscopy (CALM) for the FLIP and FRAP experiments. K.A. acknowledges Grant-in-Aid for scientific research from (grant nos. 24790425, 26713016, 18H02656, and 20H05772), Uehara Memorial Foundation, Naito Foundation, Takeda Science Foundation, and Astellas Foundation for Research on Metabolic Disorders. S.M. acknowledges financial support from the National Institutes of Health (grant nos. R01GM140440 and R01GM144378), the Pew Charitable Trust (grant no. A129837), a Bowes Biomedical Investigator award, and a gift fund from the Chan-Zuckerberg Biohub.

REFERENCES

1. Cunha BA, Burillo A, and Bouza E (2016). Legionnaires' disease. Lancet 387, 376–385. 10.1016/S0140-6736(15)60078-2. [PubMed: 26231463]
2. Qiu J, and Luo ZQ (2013). Effector translocation by the Legionella Dot/Icm type IV secretion system. Curr. Top. Microbiol. Immunol. 376, 103–115. 10.1007/82_2013_345. [PubMed: 23918176]
3. Luo ZQ, and Isberg RR (2004). Multiple substrates of the Legionella pneumophila Dot/Icm system identified by interbacterial protein transfer. Proc. Natl. Acad. Sci. USA 101, 841–846. 10.1073/pnas.0304916101. [PubMed: 14715899]
4. Qiu J, and Luo ZQ (2017). Legionella and Coxiella effectors: strength in diversity and activity. Nat. Rev. Microbiol. 15, 591–605. 10.1038/nrmicro.2017.67. [PubMed: 28713154]
5. Mukherjee S, Liu X, Arasaki K, McDonough J, Galán JE, and Roy CR (2011). Modulation of Rab GTPase function by a protein phosphocholine transferase. Nature 477, 103–106. 10.1038/nature10335. [PubMed: 21822290]
6. Arasaki K, Toomre DK, and Roy CR (2012). The Legionella pneumophila Effector DrrA Is Sufficient to Stimulate SNARE-Dependent Membrane Fusion. Cell Host Microbe 11, 46–57. 10.1016/j.chom.2011.11.009. [PubMed: 22264512]
7. Finsel I, Ragaz C, Hoffmann C, Harrison CF, Weber S, van Rahden VA, Johannes L, and Hilbi H (2013). The Legionella effector RidL inhibits retrograde trafficking to promote intracellular replication. Cell Host Microbe 14, 38–50. 10.1016/j.chom.2013.06.001. [PubMed: 23870312]
8. Hilbi H, Nagai H, Kubori T, and Roy CR (2017). Subversion of Host Membrane Dynamics by the Legionella Dot/Icm Type IV Secretion System. Curr. Top. Microbiol. Immunol. 413, 221–242. 10.1007/978-3-319-75241-9_9. [PubMed: 29536361]
9. Steinbach A, Bhadkamkar V, Jimenez-Morales D, Stevenson E, Jang GM, Krogan NJ, Swaney DL, and Mukherjee S (2024). Cross-family small GTPase ubiquitination by the intracellular pathogen Legionella pneumophila. Mol. Biol. Cell 35, ar27. 10.1091/mbc.E23-06-0260. [PubMed: 38117589]
10. Horenkamp FA, Mukherjee S, Alix E, Schauder CM, Hubber AM, Roy CR, and Reinisch KM (2014). Legionella pneumophila subversion of host vesicular transport by SidC effector proteins. Traffic 15, 488–499. 10.1111/tra.12158. [PubMed: 24483784]
11. Kalayil S, Bhogaraju S, Bonn F, Shin D, Liu Y, Gan N, Basquin J, Grumati P, Luo ZQ, and Dikic I (2018). Insights into catalysis and function of phosphoribosyl-linked serine ubiquitination. Nature 557, 734–738. 10.1038/s41586-018-0145-8. [PubMed: 29795347]
12. Bhogaraju S, and Dikic I (2016). Cell biology: Ubiquitination without E1 and E2 enzymes. Nature 533, 43–44. 10.1038/nature17888. [PubMed: 27096359]
13. Qiu J, Sheedlo MJ, Yu K, Tan Y, Nakayasu ES, Das C, Liu X, and Luo ZQ (2016). Ubiquitination independent of E1 and E2 enzymes by bacterial effectors. Nature 533, 120–124. 10.1038/nature17657. [PubMed: 27049943]
14. Bhogaraju S, Kalayil S, Liu Y, Bonn F, Colby T, Matic I, and Dikic I (2016). Phosphoribosylation of Ubiquitin Promotes Serine Ubiquitination and Impairs Conventional Ubiquitination. Cell 167, 1636–1649.e13. 10.1016/j.cell.2016.11.019. [PubMed: 27912065]
15. Black MH, Osinski A, Gradowski M, Servage KA, Paw1owski K, Tomchick DR, and Tagliabracci VS (2019). Bacterial pseudokinase catalyzes protein polyglutamylation to inhibit the SidE-family ubiquitin ligases. Science 364, 787–792. 10.1126/science.aaw7446. [PubMed: 31123136]
16. Hubber A, and Roy CR (2010). Modulation of host cell function by Legionella pneumophila type IV effectors. Annu. Rev. Cell Dev. Biol. 26, 261–283. 10.1146/annurev-cellbio-100109-104034. [PubMed: 20929312]
17. Ragaz C, Pietsch H, Urwyler S, Tiaden A, Weber SS, and Hilbi H (2008). The Legionella pneumophila phosphatidylinositol-4 phosphatebinding type IV substrate SidC recruits endoplasmic reticulum vesicles to a replication-permissive vacuole. Cell Microbiol. 10, 2416–2433. 10.1111/j.1462-5822.2008.01219.x. [PubMed: 18673369]
18. Shibata Y, Voeltz GK, and Rapoport TA (2006). Rough sheets and smooth tubules. Cell 126, 435–439. 10.1016/j.cell.2006.07.019. [PubMed: 16901774]

19. Chen S, Novick P, and Ferro-Novick S (2013). ER structure and function. Curr. Opin. Cell Biol. 25, 428–433. 10.1016/j.ceb.2013.02.006. [PubMed: 23478217]
20. Itskanov S, and Park E (2023). Mechanism of Protein Translocation by the Sec61 Translocon Complex. Cold Spring Harbor Perspect. Biol 15, a041250. 10.1101/cshperspect.a041250.
21. Quistgaard EM (2021). BAP31: Physiological functions and roles in disease. Biochimie 186, 105–129. 10.1016/j.biochi.2021.04.008. [PubMed: 33930507]
22. Wakana Y, Takai S, Nakajima KI, Tani K, Yamamoto A, Watson P, Stephens DJ, Hauri HP, and Tagaya M (2008). Bap31 is an itinerant protein that moves between the peripheral endoplasmic reticulum (ER) and a juxtanuclear compartment related to ER-associated Degradation. Mol. Biol. Cell 19, 1825–1836. 10.1091/mbc.e07-08-0781. [PubMed: 18287538]
23. Smith M, and Wilkinson S (2017). ER homeostasis and autophagy. Essays Biochem. 61, 625–635. 10.1042/EBC20170092. [PubMed: 29233873]
24. Roy CR, and Tilney LG (2002). The road less traveled: transport of Legionella to the endoplasmic reticulum. J. Cell Biol. 158, 415–419. 10.1083/jcb.200205011. [PubMed: 12147677]
25. Kotewicz KM, Ramabhadran V, Sjoblom N, Vogel JP, Haenssler E, Zhang M, Behringer J, Scheck RA, and Isberg RR (2017). A Single Legionella Effector Catalyzes a Multistep Ubiquitination Pathway to Rearrange Tubular Endoplasmic Reticulum for Replication. Cell Host Microbe 21, 169–181. 10.1016/j.chom.2016.12.007. [PubMed: 28041930]
26. Fu J, Li S, Guan H, Li C, Zhao YB, Chen TT, Xian W, Zhang Z, Liu Y, Guan Q, et al. (2024). Legionella maintains host cell ubiquitin homeostasis by effectors with unique catalytic mechanisms. Nat. Commun. 15, 5953. 10.1038/s41467-024-50311-2. [PubMed: 39009586]
27. Fu J, Zhou M, Gritsenko MA, Nakayasu ES, Song L, and Luo ZQ (2022). Legionella pneumophila modulates host energy metabolism by ADP-ribosylation of ADP/ATP translocases. Elife 11, e73611. 10.7554/eLife.73611. [PubMed: 35084332]
28. Choy A, Dancourt J, Mugo B, O'Connor TJ, Isberg RR, Melia TJ, and Roy CR (2012). The Legionella effector RavZ inhibits host autophagy through irreversible Atg8 deconjugation. Science 338, 1072–1076. 10.1126/science.1227026. [PubMed: 23112293]
29. Lehman SS, Williamson CD, Tucholski T, Ellis NA, Bouchard S, Jarnik M, Allen M, Nita-Lazar A, and Machner MP (2024). The Legionella pneumophila effector DenR hijacks the host NRas proto-oncoprotein to downregulate MAPK signaling. Cell Rep. 43, 114033. 10.1016/j.celrep.2024.114033. [PubMed: 38568811]
30. Robinson CG, and Roy CR (2006). Attachment and fusion of endoplasmic reticulum with vacuoles containing Legionella pneumophila. Cell Microbiol. 8, 793–805. 10.1111/j.1462-5822.2005.00666.x. [PubMed: 16611228]
31. Stenmark H (2009). Rab GTPases as coordinators of vesicle traffic. Nat. Rev. Mol. Cell Biol. 10, 513–525. 10.1038/nrm2728. [PubMed: 19603039]
32. Goody RS, and Itzen A (2013). Modulation of small GTPases by Legionella. Curr. Top. Microbiol. Immunol. 376, 117–133. 10.1007/82_2013_340. [PubMed: 23918171]
33. English AR, and Voeltz GK (2013). Rab10 GTPase regulates ER dynamics and morphology. Nat. Cell Biol. 15, 169–178. 10.1038/ncb2647. [PubMed: 23263280]
34. Jeng EE, Bhadkamkar V, Ibe NU, Gause H, Jiang L, Chan J, Jian R, Jimenez-Morales D, Stevenson E, Krogan NJ, et al. (2019). Systematic Identification of Host Cell Regulators of Legionella pneumophila Pathogenesis Using a Genome-wide CRISPR Screen. Cell Host Microbe 26, 551–563.e6. 10.1016/j.chom.2019.08.017. [PubMed: 31540829]
35. Fu W, Sun H, Zhao Y, Chen M, Yang X, Liu Y, and Jin W (2019). BCAP31 drives TNBC development by modulating ligand-independent EGFR trafficking and spontaneous EGFR phosphorylation. Theranostics 9, 6468–6484. 10.7150/thno.35383. [PubMed: 31588230]
36. Paquet ME, Cohen-Doyle M, Shore GC, and Williams DB (2004). Bap29/31 influences the intracellular traffic of MHC class I molecules. J. Immunol. 172, 7548–7555. 10.4049/jimmunol.172.12.7548. [PubMed: 15187134]
37. O'Connor TJ, Adepoju Y, Boyd D, and Isberg RR (2011). Minimization of the Legionella pneumophila genome reveals chromosomal regions involved in host range expansion. Proc. Natl. Acad. Sci. USA 108, 14733–14740. 10.1073/pnas.1111678108. [PubMed: 21873199]

38. Quistgaard EM, Lö w C, Moberg P, Guettou F, Maddi K, and Nordlund P (2013). Structural and biophysical characterization of the cytoplasmic domains of human BAP29 and BAP31. PLoS One 8, e71111. 10.1371/journal.pone.0071111. [PubMed: 23967155]
39. Schamel WWA, Kuppig S, Becker B, Gimborn K, Hauri HP, and Reth M (2003). A high-molecular-weight complex of membrane proteins BAP29/BAP31 is involved in the retention of membrane-bound IgD in the endoplasmic reticulum. Proc. Natl. Acad. Sci. USA 100, 9861–9866. 10.1073/pnas.1633363100. [PubMed: 12886015]
40. Iinuma T, Aoki T, Arasaki K, Hirose H, Yamamoto A, Samata R, Hauri HP, Arimitsu N, Tagaya M, and Tani K (2009). Role of syntaxin 18 in the organization of endoplasmic reticulum subdomains. J. Cell Sci. 122, 1680–1690. 10.1242/jcs.036103. [PubMed: 19401338]
41. Noack J, and Mukherjee S (2020). Make way": Pathogen exploitation of membrane traffic. Curr. Opin. Cell Biol. 65, 78–85. 10.1016/j.ceb.2020.02.011. [PubMed: 32234681]
42. Schroeder GN (2017). The Toolbox for Uncovering the Functions of Legionella Dot/Icm Type IVb Secretion System Effectors: Current State and Future Directions. Front. Cell. Infect. Microbiol. 7, 528. 10.3389/fcimb.2017.00528. [PubMed: 29354599]
43. Parlakgül G, Arruda AP, Cagampan E, Pang S, Güney E, Lee Y, Hess HF, Xu CS, and Hotamısxlıgil GS (2020). High resolution 3D imaging of liver reveals a central role for subcellular architectural organization in metabolism. Preprint at: bioRxiv. 10.1101/2020.11.18.387803
44. Hatsuzawa K, Hirose H, Tani K, Yamamoto A, Scheller RH, and Tagaya M (2000). Syntaxin 18, a SNAP receptor that functions in the endoplasmic reticulum, intermediate compartment, and cis-Golgi vesicle trafficking. J. Biol. Chem. 275, 13713–13720. 10.1074/jbc.275.18.13713. [PubMed: 10788491]
45. Arasaki K, Mikami Y, Shames SR, Inoue H, Wakana Y, and Tagaya M (2017). Legionella effector Lpg1137 shuts down ER-mitochondria communication through cleavage of syntaxin 17. Nat. Commun. 8, 15406. 10.1038/ncomms15406. [PubMed: 28504273]
46. Berger KH, and Isberg RR (1993). Two distinct defects in intracellular growth complemented by a single genetic locus in Legionella pneumophila. Mol. Microbiol. 7, 7–19. 10.1111/j.1365-2958.1993.tb01092.x. [PubMed: 8382332]
47. Zuckman DM, Hung JB, and Roy CR (1999). Pore-forming activity is not sufficient for Legionella pneumophila phagosome trafficking and intracellular growth. Mol. Microbiol. 32, 990–1001. 10.1046/j.d1365-2958.1999.01410.x. [PubMed: 10361301]
48. Arasaki K, and Roy CR (2010). Legionella pneumophila promotes functional interactions between plasma membrane syntaxins and Sec22b. Traffic 11, 587–600. 10.1111/j.1600-0854.2010.01050.x. [PubMed: 20163564]
49. Greenacre M, Groenen PJF, Hastie T, D'Enza AI, Markos A, and Tuzhilina E (2022). Principal component analysis. Nat. Rev. Methods Primers 2, 100. 10.1038/s43586-022-00184-w.
50. Yang J, Yan R, Roy A, Xu D, Poisson J, and Zhang Y (2015). The I-TASSER Suite: protein structure and function prediction. Nat. Methods 12, 7–8. 10.1038/nmeth.3213.
51. Yang J, Wang Y, and Zhang Y (2016). ResQ: An Approach to Unified Estimation of B-Factor and Residue-Specific Error in Protein Structure Prediction. J. Mol. Biol. 428, 693–701. 10.1016/j.jmb.2015.09.024. [PubMed: 26437129]
52. Waterhouse A, Bertoni M, Bienert S, Studer G, Tauriello G, Gumienny R, Heer FT, de Beer TAP, Rempfer C, Bordoli L, et al. (2018). SWISS-MODEL: homology modelling of protein structures and complexes. Nucleic Acids Res. 46, W296–W303. 10.1093/nar/gky427. [PubMed: 29788355]
53. Varadi M, Bertoni D, Magana P, Paramval U, Pidruchna I, Radhakrishnan M, Tsenkov M, Nair S, Mirdita M, Yeo J, et al. (2024). AlphaFold Protein Structure Database in 2024: providing structure coverage for over 214 million protein sequences. Nucleic Acids Res. 52, D368–D375. 10.1093/nar/gkad1011. [PubMed: 37933859]
54. Paysan-Lafosse T, Blum M, Chuguransky S, Grego T, Pinto BL, Salazar GA, Bileschi ML, Bork P, Bridge A, Colwell L, et al. (2023). InterPro in 2022. Nucleic Acids Res. 51, D418–D427. 10.1093/nar/gkac993. [PubMed: 36350672]
55. Miyamoto S, and Kollman PA (1992). Settle: An analytical version of the SHAKE and RATTLE algorithm for rigid water models. J. Comput. Chem. 13, 952–962. 10.1002/jcc.540130805.

56. Páll S, Abraham MJ, Kutzner C, Hess B, and Lindahl E (2015). Tackling Exascale Software Challenges in Molecular Dynamics Simulations with GROMACS (held in Cham: Springer International Publishing), pp. 3–27.

57. Yan Y, Tao H, He J, and Huang SY (2020). The HDOCK server for integrated protein-protein docking. Nat. Protoc. 15, 1829–1852. 10.1038/s41596-020-0312-x. [PubMed: 32269383]

58. Vaught A (1996). Graphing with Gnuplot and Xmgr: Two Graphing Packages Available under Linux (Belltown Media Linux Journal Staff).

Highlights

- *Legionella* forms a replicative vacuole (LCV) that is distinct from the host rough ER
- Host GTPases Rab 4 and Rab10 play crucial roles in LCV maturation
- *Legionella* effector Lpg1152 binds to BAP31 to facilitate LCV maturation

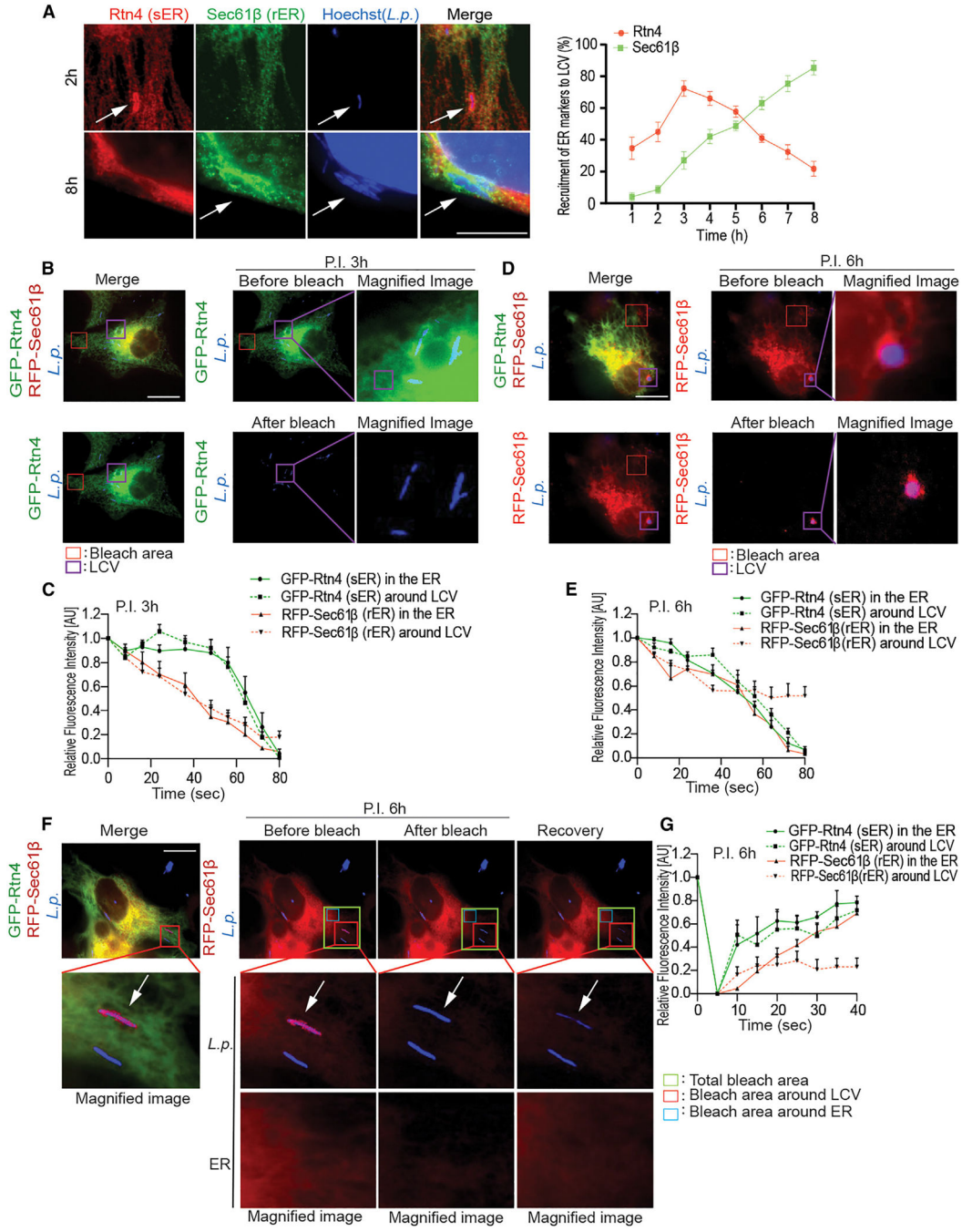

Figure 1. *L.p.* temporally associates with the sER and rER and later creates a unique ER niche independent of the host ER network

(A) HeLa Fcγ cells were infected with *L.p.* for the indicated times, stained with anti-Rtn4 (sER marker), Sec61β (rER marker) antibodies, and Hoechst (*L.p.*) for immunofluorescence analysis. Results represent three independent experiments (100 vacuoles were scored in each). Error bars represent mean ± SD. Bar, 5 μm.

(B) HeLa Fcγ cells stably expressing GFP-Rtn4 and RFP-Sec61β were infected with Halo-tagged WT *L.p.* for 3 h for FLIP. The top panel represents GFP-Rtn4 before photobleaching, and the bottom represents GFP-Rtn4 after photobleaching for 80 s. Bar, 10 μm.

(C) The graph represents the relative fluorescence intensity of GFP-Rtn4 (green lines) and RFP-Sec61β (red lines) in the ER and around LCV. Error bars represent mean ± SD. The purple and red boxes represent the area around LCV and bleach areas, respectively.
(D) HeLa Fcγ cells stably expressing GFP-Rtn4 and RFP-Sec61β were infected with WT *L.p.* for 6 h. The top panel represents RFP-Sec61β before photobleaching, and the bottom represents RFP-Sec61β after photobleaching. The purple and red boxes represent the area around the LCV and bleach areas, respectively. Bar, 10 μm.
(E) The graph represents the relative fluorescence intensity of GFP-Rtn4 (green lines) and RFP-Sec61β (red lines) in the ER and around LCV.
(F) HeLa Fcγ cells stably expressing GFP-Rtn4 and RFP-Sec61β were infected for 6 h, and RFP-Sec61β was photobleached for FRAP. The green box represents the total area of bleach. The red and blue boxes represent the bleached area around the LCV and the ER, respectively. White arrows represent the area around LCV. Bar, 10 μm.
(G) The graph represents the relative fluorescence intensity of GFP-Rtn4 (green lines) and RFP-Sec61β (red lines) in the ER and around LCV. Error bars represent mean ± SD.

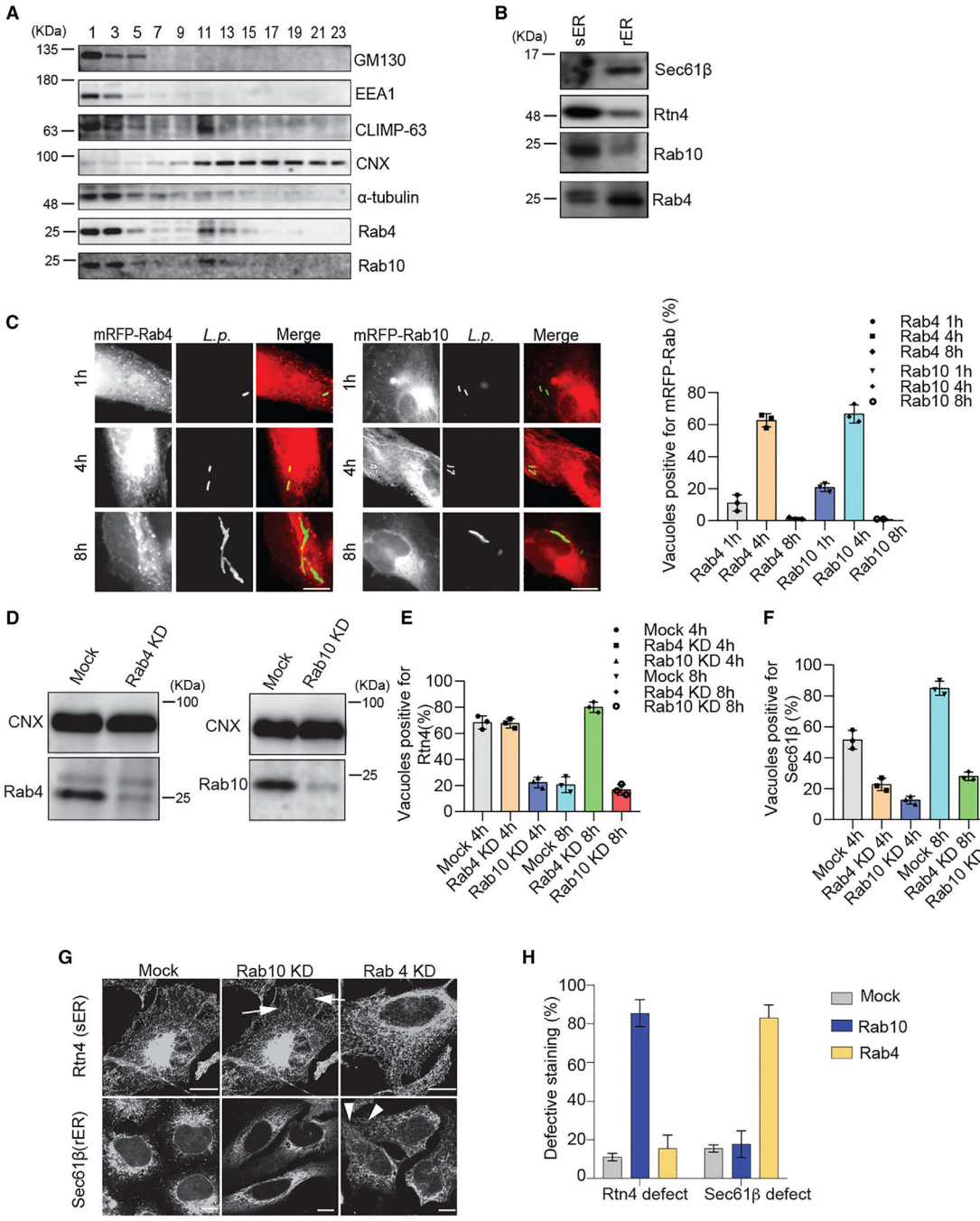

Figure 2. Rab4 and Rab10 facilitate the transition of the LCV from an sER to an rER identity

(A) HeLa Fcγ cells were subjected to subcellular fractionation, and immunoblot analysis was done against the indicated proteins.

(B) Sucrose gradient fractionation was done to obtain the sER and rER fractions and immunoblotted against indicated antibodies.

(C) HeLa Fcγ cells expressing mRFP-Rab4 or mRFP-Rab10 were infected with *L.p.* for the indicated times, stained with *L.p.* for immunofluorescence analysis, and the vacuoles positive for mRFP-Rab4 or -Rab10 were quantified. Bar, 5 μm. The purple box represents

the magnified image. Results represent three independent experiments (100 vacuoles were scored in each). Error bars represent mean ± SD.

(D) HEK293 Fcγ cells were transfected with either mock, Rab4, or Rab10 siRNA for 72 h, and cell extracts were immunoblotted against the indicated antibodies.

(E and F) HeLa Fcγ cells were silenced for Rab4 or Rab10 for 72 h, infected with *L.p.* for 4 and 8 h, and the vacuoles positive for Rtn4 or Sec61β were counted. Results represent three independent experiments, and statistical significance was measured using one-way ANOVA (100 vacuoles were scored in each experiment). Bars represent mean ± SD.

(G) HeLa Fcγ cells were silenced with Rab4 and Rab10 siRNA, and the ER morphology was observed by immunofluorescence analysis. Bars, 5 μm. Arrows indicate disruption of the sER tubular network. Arrowheads indicate diffusion of rER to the cell periphery.

(H) Triplicate experiments (30 cells for each condition) from 3G were quantitated and are shown as a histogram. Bars represent mean ± SD.

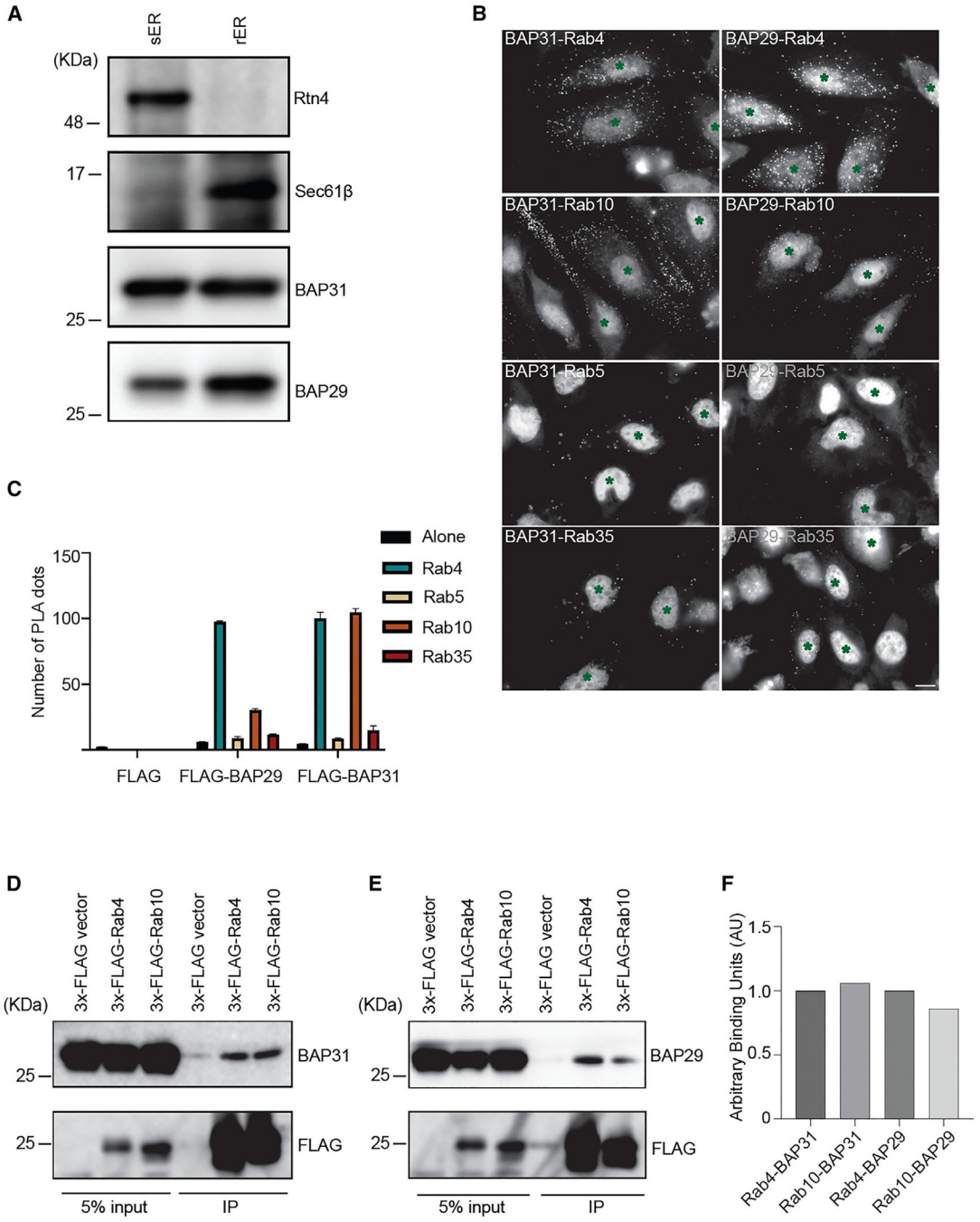

Figure 3. BAP31 binds to Rab4 and Rab10, while BAP29 interacts with Rab4

(A) The membranes of sER and rER fractions were collected by centrifugation and subjected to immunoblotting against the indicated antibodies.

(B) HeLa Fcγ cells expressing GFP vector and either 3x-FLAG-Rab4, -Rab5, -Rab10, or -Rab35 were fixed, proximity ligation assay (PLA) was performed using the indicated antibodies, and the number of PLA dots was quantified. Bar, 5 μm. Green asterisks indicate the cells expressing GFP, implicating the expression of 3x-FLAG constructs.

(C) Results from 3B are representative of three independent experiments, and statistical significance was achieved using one-way ANOVA (PLA dots in 25 cells expressing GFP were scored in each experiment). Error bars represent mean ± SD. ****$p < 0.0001$.
(D and E) HEK293 Fcγ cells were transfected with the indicated plasmids, and cell extracts were subjected to immunoprecipitation assay using the anti-FLAG antibody and immunoblotted against the indicated antibodies.
(F) Results from 3D and 3E are quantitated and shown as a histogram.

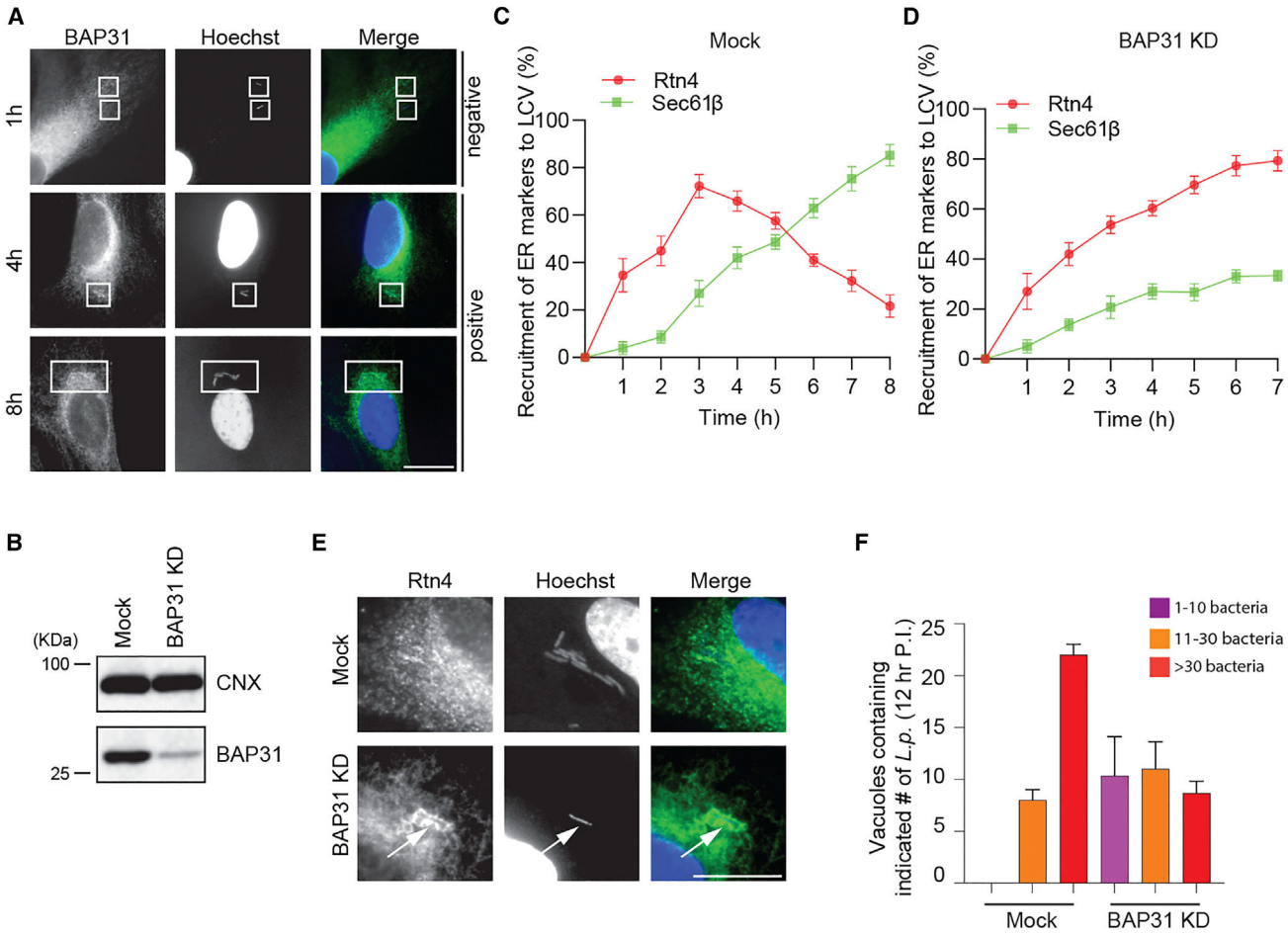

Figure 4. BAP31 is required for the sER to rER transition and efficiently replicate *Legionella*

(A) HeLa Fcγ cells were infected with *L.p.* for the indicated time, fixed, and stained with anti-BAP31 antibody and Hoechst 33342. White boxes indicate the LCV.

(B) HeLa Fcγ cells were transfected with either mock or BAP31 siRNA for 72 h and immunoblotted against the indicated antibodies.

(C and D) Mock-treated or BAP31-silenced HeLa Fcγ cells were infected with *L.p.* for the indicated time, fixed, and stained with anti-Rtn4 or -Sec61β antibodies and DAPI, and the vacuoles were quantified. Results are representative of three independent experiments (100 vacuoles were scored in each experiment). Bars represent mean ± SD.

(E) HeLa Fcγ cells were silenced with either mock or BAP31 for 72 h, followed by infection with *L.p.* for 8 h. Post infection, cells were fixed and stained with anti-Rtn4 antibody and Hoechst for immunofluorescence analysis. Bar, 5 μm.

(F) HeLa Fcγ cells were silenced with either mock or BAP31 for 72 h, followed by infection with *L.p.* for 12 h at an MOI of 2. Post infection, cells were fixed and stained with anti-*Legionella* antiserum for detection of extracellular bacteria, then permeabilized and further stained with DAPI for detection of intracellular bacteria. Bar, 5 μm. The graph shows the percentage of vacuoles containing a single bacterium, 1–10 bacteria, 11–30 bacteria, and ≥31 bacteria in a single vacuole. Data are representative of three independent experiments

(30 vacuoles were scored in each experiment). Results are shown as the mean ± SD. ***$p < 0.001$.

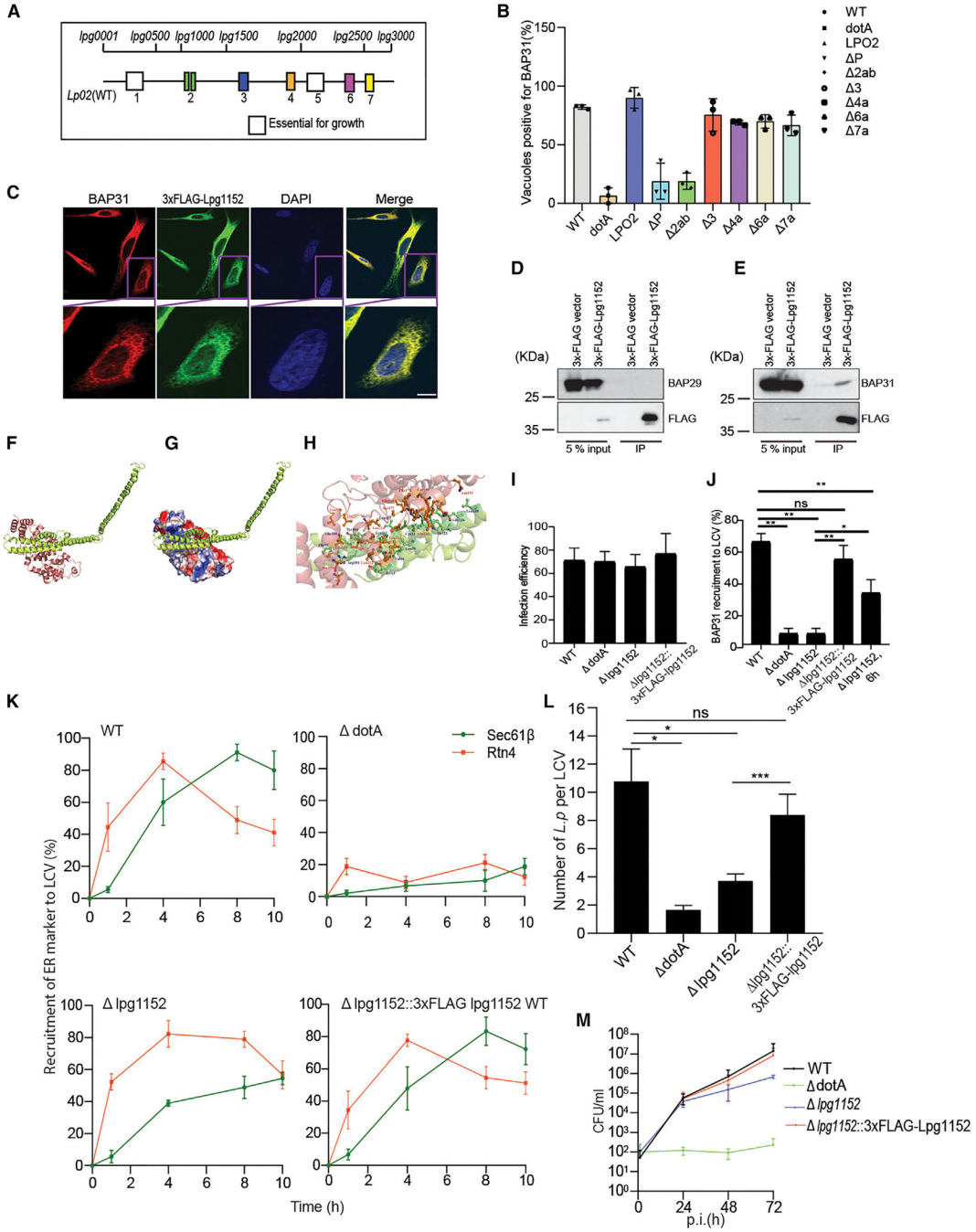

Figure 5. Lpg1152 brings BAP31 to LCVs and is required for optimal LCV maturation and replication of *Legionella*

(A) Schematic representation of the chromosomal organization of genomic islands of *L.p.*

(B) HeLa Fcγ cells were infected with the indicated genomic island deletion mutant *L.p.* strains for 4 h and processed for immunofluorescence against BAP31 antibody. The histogram represents the percentage of vacuoles positive for BAP31 post infection with different *L.p.* strains.

(C) HeLa Fcγ cells were transfected with 3xFLAG-Lpg1152 plasmid and processed for immunofluorescence microscopy using FLAG (green) and BAP31 (red) antibodies. Nuclei were stained with DAPI. Bar, 10μm.

(D and E) HEK293 Fcγ cells were transfected with the indicated plasmids. Cell extracts were subjected to immunoprecipitation assay post transfection with anti-FLAG antibody and immunoblotted against the indicated antibodies.

(F) The docked model complex of Lpg1152 (deep salmon) and BAP31 (green).

(G) The electrostatic potential surface of Lpg1152 is shown bound with BAP31 (green).

(H) Interacting residues of Lpg1152 (orange, ball-stick) and BAP31 (lime, ball-stick) at the protein-protein interface.

(I) HeLa Fcγ cells were infected with the indicated *L.p.* strains. Histograms represent the infection efficiency, i.e., the percentage of infected cells at MOI 10 1.5 h after infection (n = 200 per triplicate experiment).

(J) HeLa Fcγ cells were infected with the indicated strains of *L.p.* for the indicated time points. Following infection, LCV positive for BAP31 was scored using immunofluorescence analysis.

(K) HeLa Fcγ cells were infected with the indicated strain, and the Rtn4- and Sec61β-positive vacuoles were scored using immunofluorescence. Graphs represent the percentage recruitment of Rtn4 and Sec61β at the indicated time points post infection.

(L) HeLa Fcγ cells were infected with the indicated *L.p.* strains, and the number of *L.p.* per LCV was counted 8 h after infection (n = 30 per triplicate experiment).

(M) U937 cells were infected with the indicated *L.p.* strains for 1 h, and colony-forming units (CFU) were counted at the indicated time after infection. Data represent three independent experiments, and statistical significance was carried out with a Student’s t test. Bar represents mean ± SEM.

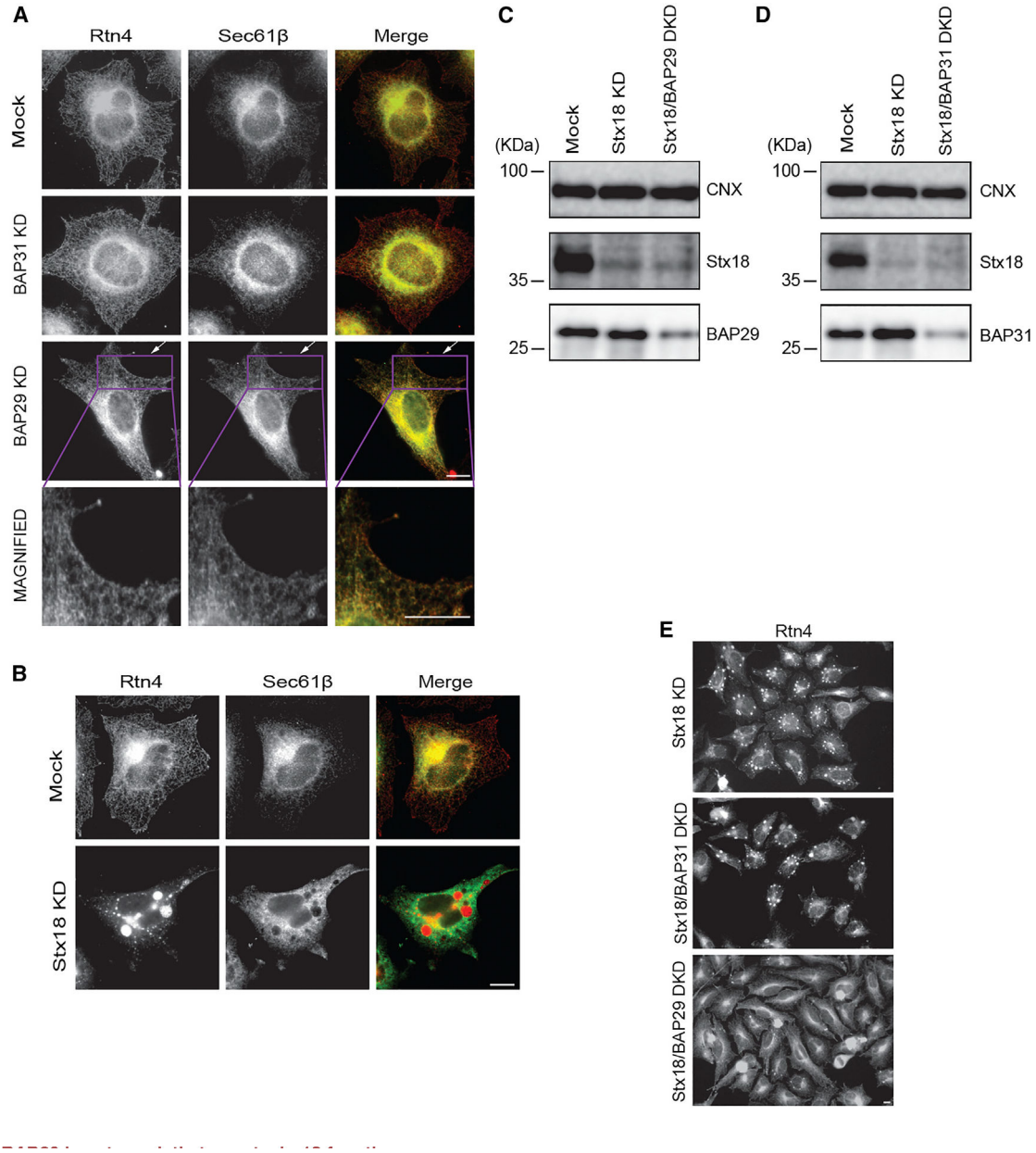

Figure 6. BAP29 is antagonistic to syntaxin 18 function

(A) HeLa Fcγ cells were silenced with mock, BAP31, or BAP29 siRNA for 72 h. Post silencing, cells were fixed and stained with anti-Rtn4 and Sec61β antibodies and were subjected to immunofluorescence imaging. Bar, 5 μm. White arrows indicate Sec61β localization to the cell periphery.

(B) HeLa Fcγ cells were silenced with either mock or Stx-18 siRNA for 72 h. Post silencing, cells were fixed and stained with anti-Rtn4 and anti-Sec61β antibodies. Bar, 5 μm.

(C and D) HeLa Fcγ cells were silenced for Stx18 alone or a combination of Stx18/BAP31 or Stx18/BAP29 siRNA. Following single or double silencing, cell extracts were prepared and immunoblotted against the indicated antibodies.

(E) HeLa Fcγ cells were silenced for Stx18 alone, Stx18/BAP31, or Stx18/BAP29; following single or double silencing, cells were fixed and stained with an anti-Rtn4 antibody for immunofluorescence analysis. Bar, 5 μm.

KEY RESOURCES TABLE

REAGENTor RESOURCE	SOURCE	IDENTIFIER
Antibodies		
Anti-FLAG rabbit polyclonal antibody	Sigma	Cat# F7425
Anti-FLAG mouse monoclonal antibody	Sigma	Cat# F3165
Anti-Rtn4 goat polyclonal antibody	CiteAb	Cat# sc-11027
Anti-Sec61β rabbit polyclonal antibody	Proteintech	Cat# 14846-1-AP
Anti-GM130 mouse monoclonal antibody	BD Biosciences	Cat# 610823
Anti-GFP rabbit polyclonal antibody	Thermo Fisher Scientific	Cat# A-6455
Anti-CLIMP-63 mouse monoclonal antibody	Enzo	Cat# ALX-804-604
Anti-CNX mouse monoclonal antibody	BD Biosciences	Cat# 610524
Anti-Rab4 rabbit polyclonal antibody	Cell signaling	Cat# 2167
Anti-Rab10 rabbit polyclonal antibody	Cell signaling	Cat# 4262
Anti-α-tubulin mouse monoclonal antibody	Sigma	Cat# T6074
Anti-BAP29 rabbit polyclonal antibody	Proteintech	Cat# 15796-1-AP
Anti-BAP31 rabbit polyclonal antibody	Proteintech	Cat# 11200-1-AP
Anti-Stx18	Hatsuzawa et al.[44]	N/A
Anti-EEA1 mouse monoclonal antibody	BD Biosciences	Cat# 610457
Anti-*Legionella* rabbit polyclonal antiserum	Arasaki et al.[45]	N/A
Anti-*Legionella* mouse polyclonal antiserum	Arasaki et al.[45]	N/A
Anti-*Legionella* rabbit polyclonal antiserum	Invitrogen	Cat #PA1-7227
Anti-Sec61β rabbit polyclonal antibody	Proteintech	Cat# 15087-1-AP
Anti-Rtn4 rabbit polyclonal antibody	Abcam	Cat# ab47085
Alexa Flour 488-conjugated donkey anti-rabbit antibody	Thermo Fisher Scientific	Cat# A21206
Alexa Flour 594-conjugated donkey anti-goat antibody	Thermo Fisher Scientific	Cat# A11058
Alexa Fluor 488-conjugated goat anti-rabbit antibody	Thermo Fisher Scientific	Cat# A11034
Alexa Fluor 594conjugated goat anti-rabbit antibody	Thermo Fisher Scientific	Cat# A11037
Alexa Fluor 594conjugated goat anti-mouse antibody	Thermo Fisher Scientific	Cat# A11032
Alexa Fluor 350conjugated donkey anti-mouse antibody	Thermo Fisher Scientific	Cat# A10035
Anti-Flag M2 mouse monoclonal antibody	Sigma	Cat# F1804
Alexa fluor 488-conjugated goat anti-rabbit IgG antibody	Life Technologies	Cat# a11034
Alexa fluor 633-conjugated goat anti-mouse antibody	Life Technologies	Cat# a21052
Anti-GST Tag mouse monoclonal antibody	Proteintech	Cat# 66001-2-Ig
Anti-MBP Tag mouse monoclonal antibody	Proteintech	Cat# 66003-1-Ig
Bacterial and virus strains		
Legionella pneumophila Philadelphia-1 WT (*Lp01*)	Berger and Isberg.[46]	N/A
Legionella pneumophila Philadelphia-1 *ΔicmV ΔdotA* (*ΔdotA*)	Zuckman et al.[47]	N/A
Legionella pneumophila Philadelphia-1 *Δlpg1152*(*Δlpg1152*)	This study	N/A
Legionella pneumophila Philadelphia-1 *Δlpg1152::*3xFLAG-Lpg1152	This study	N/A
Legionella pneumophila Philadelphia-2 *WT* (*Lp02*)	O'Connor et al.[37]	N/A

REAGENTor RESOURCE	SOURCE	IDENTIFIER
Legionella pneumophila Philadelphia-2 *Δpentuple* (*ΔP*)	O'Connor et al.[37]	N/A
Legionella pneumophila Philadelphia-2 *Δ2a,b*	O'Connor et al.[37]	N/A
Legionella pneumophila Philadelphia-2 *Δ3*	O'Connor et al.[37]	N/A
Legionella pneumophila Philadelphia-2 *Δ4*	O'Connor et al.[37]	N/A
Legionella pneumophila Philadelphia-2 *Δ6*	O'Connor et al.[37]	N/A
Legionella pneumophila Philadelphia-2 *Δ7*	O'Connor et al.[37]	N/A
Escherichia coli DH5α	TOYOBO	Cat# DNA-903
Escherichia coli BL21(DE3)	New England BioLabs®	Cat# C2527I
Chemicals, peptides, and recombinant proteins		
leupeptine	Peptide Institute	Cat# 4041
pepstatin A	Peptide Institute	Cat# 4397
aprotinin	Roche	Cat# 10236624001
SlowFade™ Diamond Antifade Mountant with DAPI	Thermo Fisher Scientific	Cat# S36964
LipofectAmine2000	Thermo Fisher Scientific	Cat# 11668500
FLAG M2 agarose beads	Sigma	Cat# A2220
Glutathione Sepharose™ 4B beads	GE Healthcare	Cat# 17-0756-05
Amylose resin	New England BioLabs®	Cat# E8021S
3x-FLAG peptide	Sigma	Cat# F4799
NucleoBond Xtra Midi	Takara	Cat# U0410C
Hoechst 33342	Life Technologies	Cat# H3570
Mirus TransIT-TKO Transfection reagent	mirusbio	Cat# MIR 2150
IPTG (Isopropyl-β-D-thiogalactopyranoside)	UBPBio	Cat# P1010-25
Lysozyme	Research Products International	Cat# L38100-1.0
PMSF (Phenylmethanesulfonyl fluoride)	Sigma	Cat# P7626
DL-Dithiothreitol	Sigma	Cat# D9779-5G
Recombinant GST-BAP31	This study	N/A
Recombinant MBP-Lpg1152	This study	N/A
Critical commercial assays		
Duolink *In Situ* Detection Reagents Red	Sigma	Cat# DUO92008-100RXN
Duolink *In Situ* PLA Probe Anti-Mouse MINUS	Sigma	Cat# DUO92004-100RXN
Duolink *In Situ* PLA Probe Anti-Rabbit PLUS	Sigma	Cat# DUO92002-100RXN
Duolink *In Situ* PLA Wash Buffers, Fluorescence	Sigma	Cat# DUO82049
Experimental models: Cell lines		
Human: HEK293-FcγRII	Arasaki and Roy.[48]	N/A
Human: HeLa-FcγRII	Arasaki et al.[45]	N/A
Human: U937 cells	Gift from Dr. Michael Bassik	N/A
Human: HeLa Fcγ cells stably expressing GFP-Rtn4 and RFP-Sec61β	This study	N/A

REAGENTor RESOURCE	SOURCE	IDENTIFIER
Oligonucleotides		
Primer and siRNAs	See Table S2	N/A
Recombinant DNA		
Plasmids	See Table S1	N/A
Software and algorithms		
ImageJ	Schneider et al.[49]	https://imagej.nih.gov/ij/
GraphPad Prism	GraphPad	https://www.graphpad.com/features
LumiVision PRO 400 EX	AISIN	
GROMOS96 43a1 force field	GROMOS96	https://www.scienceopen.com/document?vid=772e5dd0-5e5a-4541-98b6-d8f483bc2db8
GROMACS 5.1.2	GROMACS	https://link.springer.com/chapter/10.1007/978-3-319-15976-8_1
Steepest descent integrator	Debye, 1909	https://zenodo.org/records/2397260
Principal component analysis	Greenacre et al.[49]	https://www.nature.com/articles/s43586-022-00184-w#:~:text=Principal%20component%20analysis%20is%20a,variance%20of%20all%20the%20variables.
HDOCK server	Huang Lab	http://hdock.phys.hust.edu.cn/
XMGrace	Grace Development Team	https://plasma-gate.weizmann.ac.il/Grace/
PyMOL	Schrodinger	https://www.pymol.org/
Endnote 20	Endnote	https://endnote.com/